Supporting Information

“Clickable” Organic Electrochemical Transistors

Gonzalo E. Fenoy,[1,2] Roger Hasler,[1] Felice Quartinello,[3] Waldemar A. Marmisollé,[2] Christoph Lorenz,[4] Omar Azzaroni,[2*] Peter Bäuerle,[4*] Wolfgang Knoll[1,5*]*

[1] *AIT Austrian Institute of Technology GmbH, Konrad-Lorenz Straße 24, 3430 Tulln an der Donau, Austria*

[2] *Instituto de Investigaciones Fisicoquímicas Teóricas y Aplicadas, Departamento de Química, Facultad de Ciencias Exactas, Universidad Nacional de La Plata – CONICET, 64 and 113, 1900 La Plata, Argentina.*

[3] *Department of Agrobiotechnology, IFA-Tulln, Institute of Environmental Biotechnology, Konrad-Lorenz-Straße 20, 3430 Tulln an der Donau, Austria.*

[4] *Institute for Organic Chemistry II and Advanced Materials, University of Ulm, Albert-Einstein-Allee 11, 89081 Ulm, Germany.*

[5] *Department of Scientific Coordination and Management, Danube Private University, 3500 Krems, Austria.*

[*]E-mail: Gonzalo.Fenoy@ait.ac.at (G.E.F); Azzaroni@inifta.unlp.edu.ar (O.A.); Peter.Baeuerle@uni-ulm.de (P.B.); Wolfgang.Knoll@ait.ac.at (W.K.)

Table of Contents

Supporting Information **1**
Materials and Methods **3**
Reagents and materials 3
Characterization of EDOT-N_3 3
Further electrochemistry measurements 3
Optical Microscope measurements 3
FO probes fabrication 3
AFM measurements 4
ATR-FTIR measurements 4
Supplementary Data **5**
NMR spectra of EDOT-N_3 5
Optimization of the OECTs obtention protocol 7
OECTs parameters computing 12
Comparison of the obtention methods 13
Reproducibility of the SDS-based obtention protocol 15
PEDOT and PEDOT-N_3 comparison 16
PEDOT-N_3-OECTs characterization 17
Click of redox probes and control experiments 21
FO-SPR measurements 24
Clicking of biotin and avidin recognition on OECTs 29
Thrombin sensing experiments 31
References **33**

Materials and Methods

Reagents and materials

KCl, sodium dodecyl sulfate (SDS), ferrocene, acetonitrile (ACN), tetrabutylammonium hexafluorophosphate ($TBAPF_6$), 3,4-ethylenedioxythiophene (EDOT, 97%), dimethyl sulfoxide (DMSO), tris[(1-benzyl-1H-1,2,3-triazol-4-yl)methyl]amine (TBTA, 97%), $CuSO_4$ x$5H_2O$, *tert*-butanol (*t*-butanol), sodium ascorbate (NaAsc), N-(3-butynyl)phthalimide (N-But, 97%), and H_2O_2 were obtained from Sigma-Aldrich. $HClO_4$ (20%) was obtained from Fluka. Phosphate buffer saline (PBS) tablets were obtained from VWR. Ethynylferrocene (Et-Fc, 97%) was obtained from abcr. Acetylene-PEG_4-Biotin was obtained from Jena Bioscience. Streptavidin-Horseradish Peroxidase conjugate (1 mg/mL, 0.05M HEPES, 0.1M Na_2SO_4, pH 6.8, preservative) was obtained from Merck. NeutrAvidin protein (60 kDa) was purchased from Thermo Fisher Scientific. The dibenzocyclooctyne (DBCO)-modified thrombin-specific HD22 aptamer (sequence DBCO- 5´-TEG-TTTT TAG TCC GTG GTA GGG CAG GTT GGG GTG ACT-3´, M_w = 12.5 kDa) was custom synthesized by Integrated DNA Technologies. Thrombin purified from human plasma (M_W = 37 kDa) was purchased from Enzo Life Sciences. All solutions were prepared with Milli-Q water.

Au interdigitated microelectrodes (IDE-3, 5/5 μm gap/electrode), a Ag/AgCl reference electrode, a Pt counter electrode and a batch cell accessory were obtained from Micrux.

Characterization of EDOT-N_3

GC/EI-MS (70 eV): t_R = 12.75 min, *m/z* (%) = 197(100) [M^+], 169(15) [M^+-N_2], 141(45) [M^+-N_3]; ESI-MS: *m/z*: [M^+]: calcd. for $C_7H_7N_3O_2S$: m/z = 197.2; found: 197.15.

Elemental analysis for $C_7H_7N_3O_2S$ (*M*w 197.2), calcd (%) C 42.63, H 3.58, N 21.31, found C 42.87, H 3.65, N 21.22.

Further electrochemistry measurements

For the organic solvent measurements, a Ag/Ag^+ electrode was used as RE and a Pt wire as CE. The electrolyte solution was 0.1M $TBAF_6$ in ACN. The electrolyte was thoroughly bubbled with N_2 prior to the measurements. For the "electro"clicking procedure, the electrolyte employed was DMF and the same setup was employed (see **Click chemistry protocols Section**).

Optical Microscope measurements

Optical microscope images were obtained with an Olympus BX51M Microscope.

FO probes fabrication

Fiber optic (FO) probes were fabricated according to a previously reported procedure.[1] In brief, TECS-clad step-index multimode fibers (Thorlabs Inc.), with a numerical aperture of 0.39 and a core diameter of 1000 μm were cut to a length of 6.5 cm. At one end, a surface plasmon resonance (SPR)-sensitive zone (1 cm length) was constructed by removing the jacket layer with a stripping tool and the cladding layer by dissolution in acetone. The SPR-zone of the tip was further cleaned with Milli-Q water and isopropanol and blow dried under a flow of N_2. As-prepared tips were homogenously sputter-coated with 50 nm of gold and stored under Argon until further usage.

AFM measurements

AFM measurements were performed in tapping mode with a PicoPlus AFM microscope (Molecular Imaging, Agilent Technologies, Germany). PPP-NCHR-50 tips were employed (Nanosensors, Switzerland). The obtained images were processed with the Gwyddion software (gwyddion.net).

ATR-FTIR measurements

Fourier transform infrared spectroscopy in the attenuated total reflection mode (ATR-FTIR) spectra were recorded employing a PerkinElmer Spectrum 100 spectrometer (USA) equipped with a diamond ATR crystal and using a resolution of 2 cm^{-1} for 48 scans. The spectra were normalized for data processing.

Supplementary Data

NMR spectra of EDOT-N_3

NMR spectra were recorded on an Avance 400 spectrometer (^{1}H NMR: 400 MHz, ^{13}C NMR: 101 MHz): ^{1}H NMR ($CDCl_3$): δ = 6.36 (AB-system, J_{AB} = 3.7 Hz, 2H, Th), 4.32 (m, 1H, C*H*O), 4.20 (dd, J_1 = 11.7 Hz, J_2 = 2.3 Hz, 1H, CH_2-O), 4.05 (dd, J_1 = 1.7 Hz, J_2 = 6.9 Hz,1H, CH_2-O), 3.58 (dd, J_1 = 13.1 Hz, J_2 = 6.0 Hz, 1H, CH_2-N_3), 3.49 (dd, J_1 = 13.1 Hz, J_2 = 5.2 Hz,1H, CH_2-N_3) ppm; ^{13}C NMR ($CDCl_3$): δ = 141.0, 140.6, 100.2, 100.0, 72.4, 65.7, 50.5 ppm.

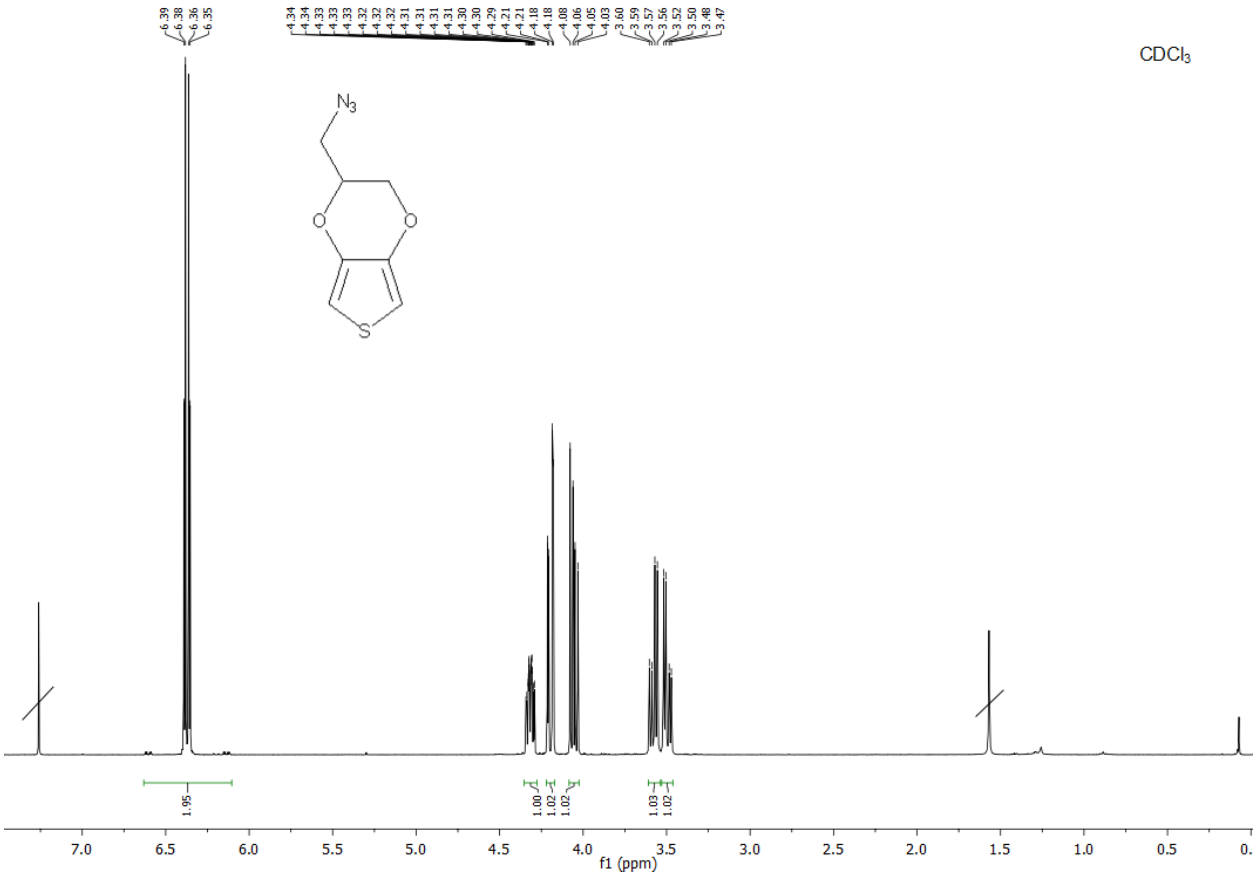

Figure S1: ^{1}H-NMR spectrum in of EDOT-N_3 in $CDCl_3$.

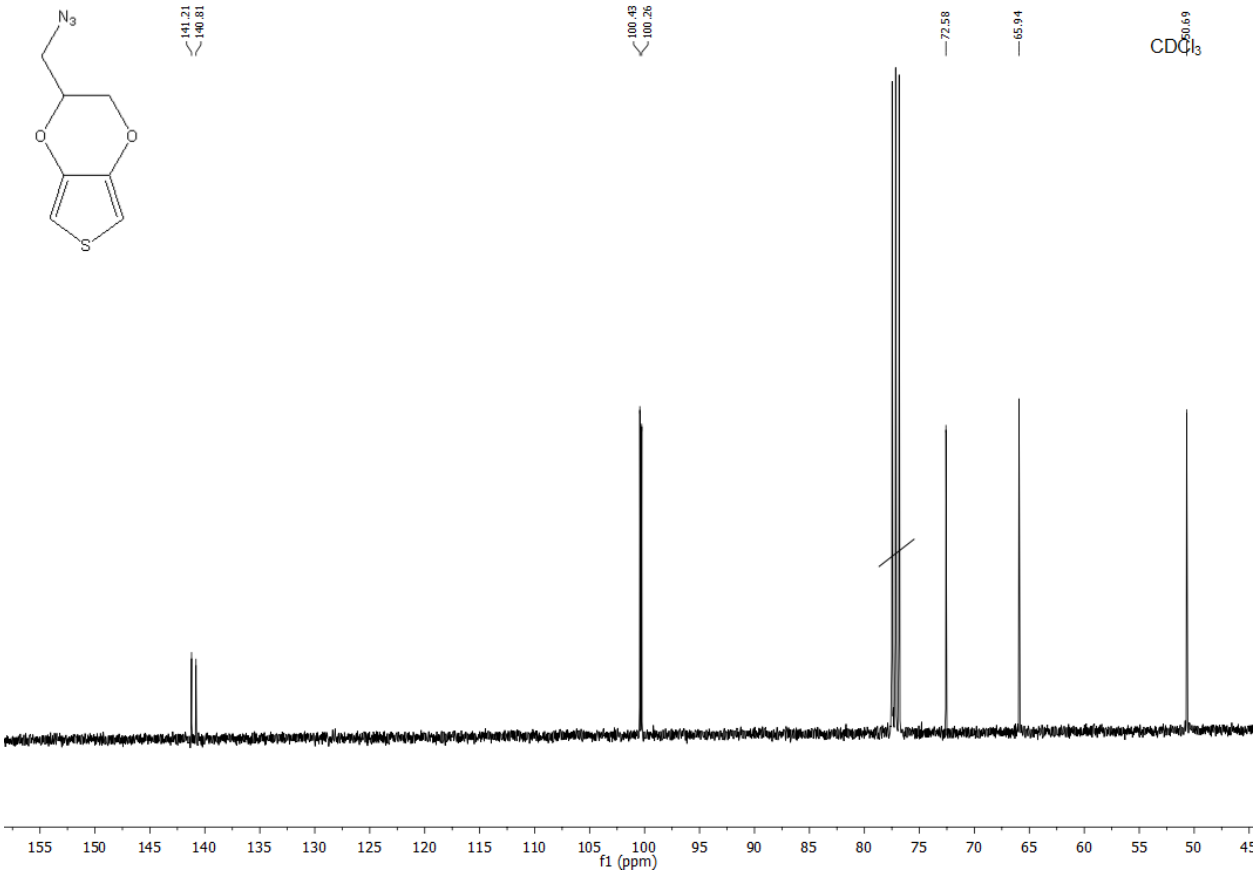

Figure S2: ^{13}C-NMR spectrum in of EDOT-N_3 in $CDCl_3$.

Optimization of the OECTs obtention protocol

Electropolymerization in ACN

The preparation of the devices was performed by electropolymerization employing a 10 mM EDOT-N_3 solution in $TBAF_6$ 0.1M in ACN, according to a previously reported protocol.[2] The anodic potential limit of the electropolymerization was varied from 1.3 V to 1.5 V in order to study its effect on the polymer film obtained. Data for 1.4 V is shown in **Figure S3**.

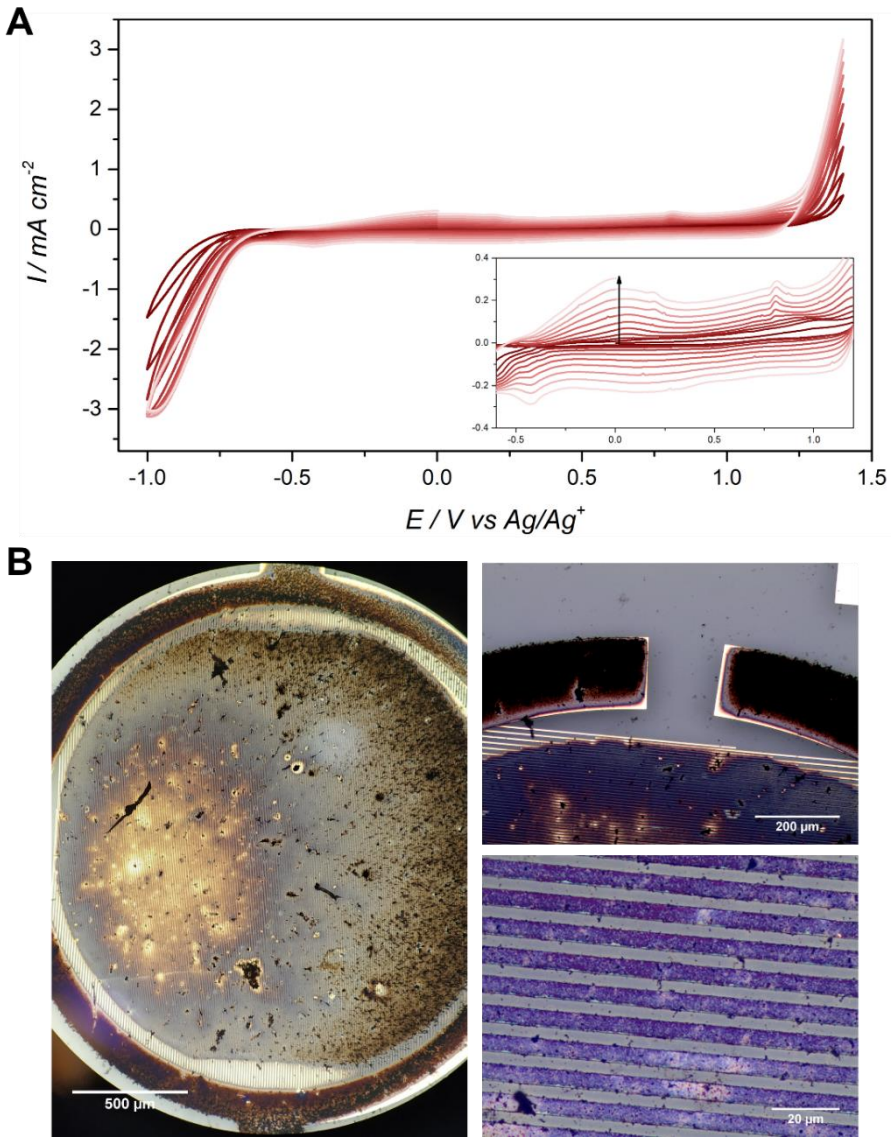

Figure S3. Voltammograms for the electropolymerization of PEDOT-N_3 on the IDEs (ACN, $TBAF_6$ 0.1M, EDOT-N_3 10 mM, 40 mV/s, 10 cycles) **(A)**. Optical micrographs of the obtained OECTs at different magnifications **(B)**.

Next, the anodic potential limit was increased to 1.5 V (**Figure S4**). It is observed that thicker PEDOT-N_3 films are obtained upon this electropolymerization procedure.

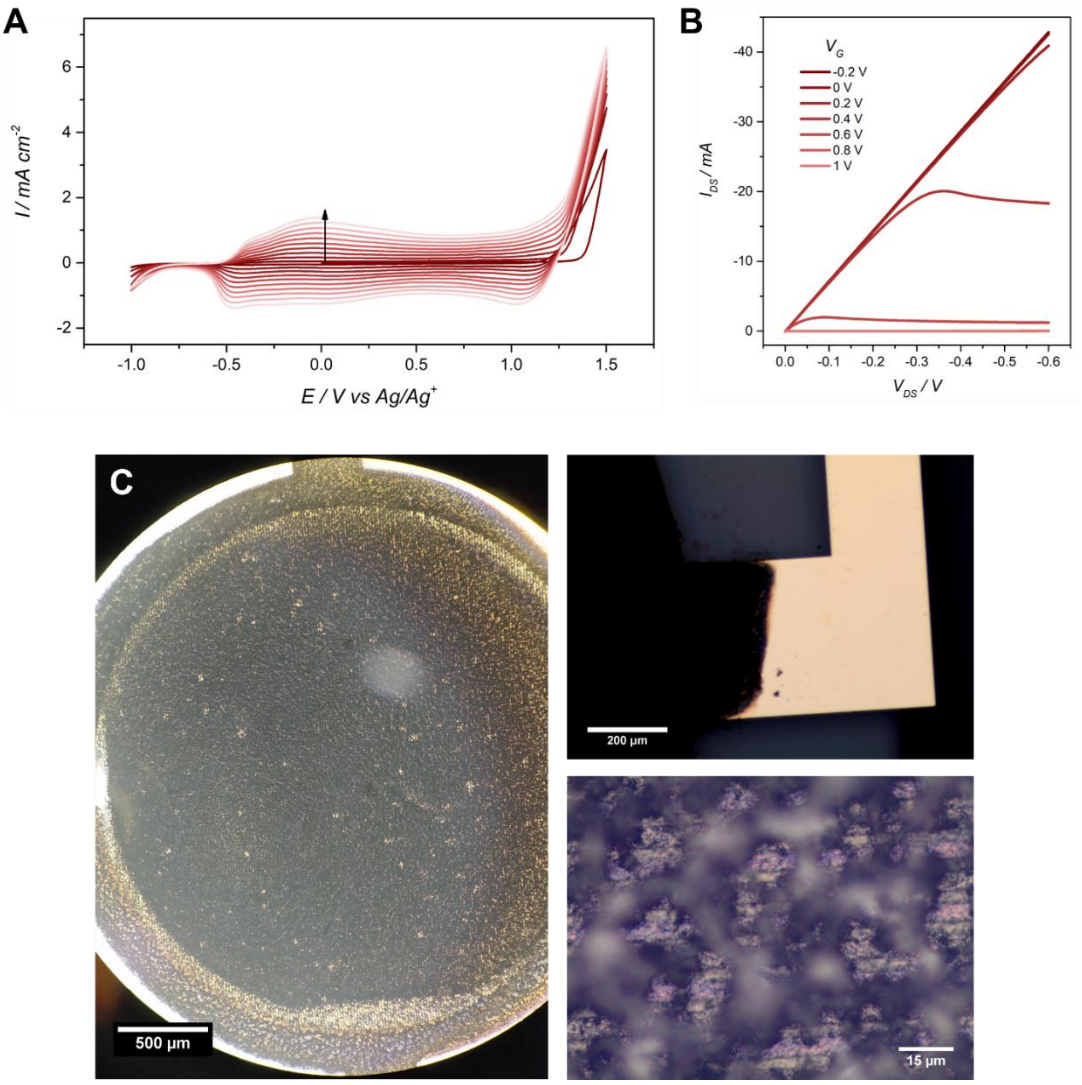

Figure S4. Voltammograms for the electropolymerization of PEDOT-N_3 on the IDEs (ACN, $TBAF_6$ 0.1M, EDOT-N_3 10 mM, 40 mV/s, 10 cycles) **(A)**. Output curves for the obtained OECTs (1xPBS) **(B)**. Optical micrographs of the obtained OECTs at different magnifications **(C)**.

When the anodic potential limit employed was 1.3 V (**Figure S5**), very thin PEDOT-N_3 films were obtained. In addition, the transistors were shown to degrade upon the continuous measuring of transfer characteristics, as shown in **Figure S5(B)**. This behavior was not observed in transistors prepared with the other preparation protocols.

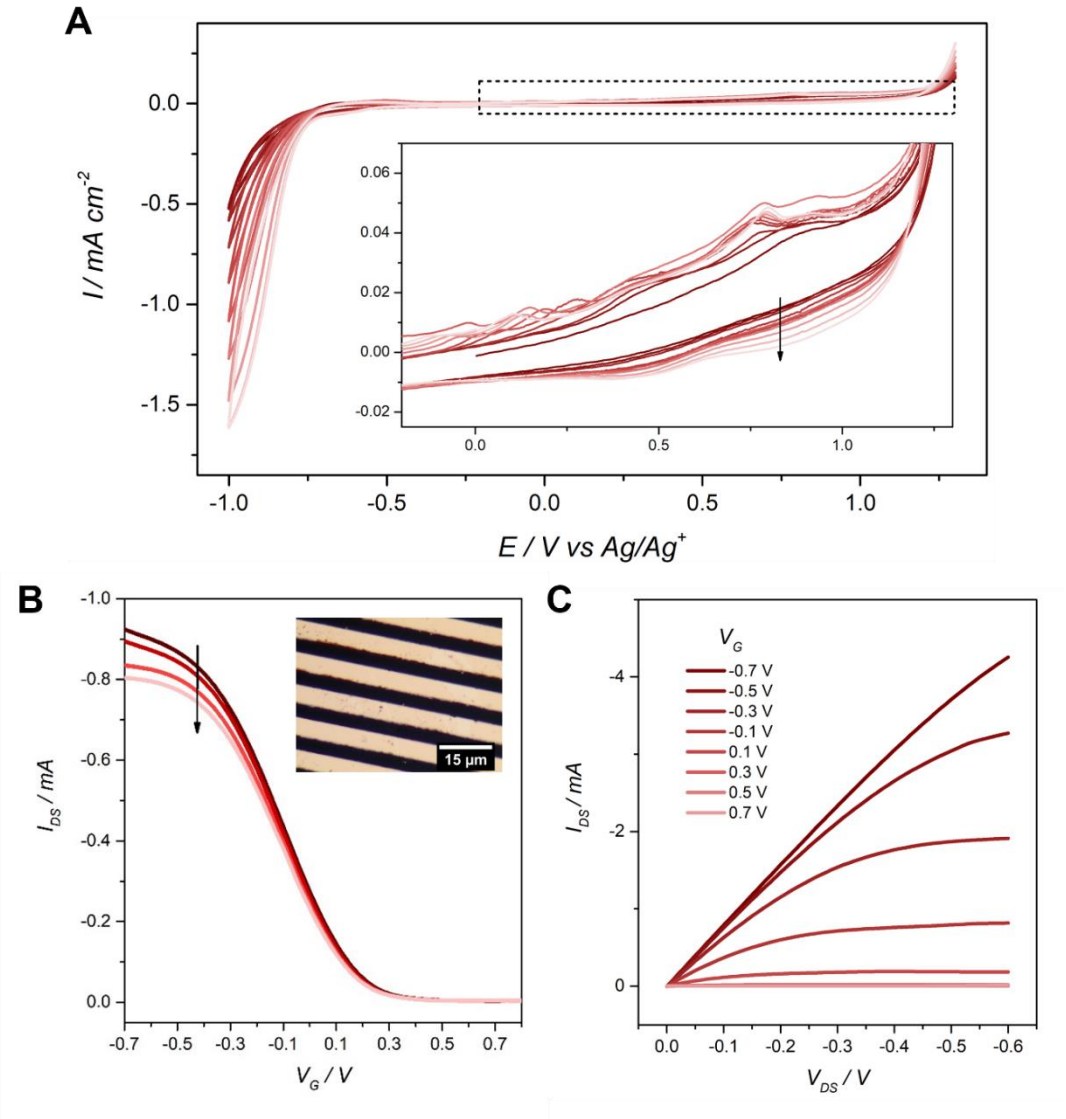

Figure S5. Voltammograms for the electropolymerization of PEDOT-N_3 on the IDEs (ACN, $TBAF_6$ 0.1M, EDOT-N_3 10 mM, 40 mV/s, 10 cycles) **(A)**. Subsequent (1 to 4, indicated by arrow) transfer characteristic curves of the obtained PEDOT-N_3 OECT (V_{DS} = -0.1 V, 1xPBS). The inset shows an optical micrograph of the obtained OECT **(B)**. Output curves for the obtained OECTs (1xPBS) **(C)**.

Electropolymerization in $HClO_4$

The obtention of the devices was also performed in an acidic solution ($HClO_4$ 0.1M, 10 mM EDOT) (**Figure S6**) according to a previously reported protocol.[3] It is observed that the films obtained under these conditions are thinner and more homogeneous than those obtained in ACN.

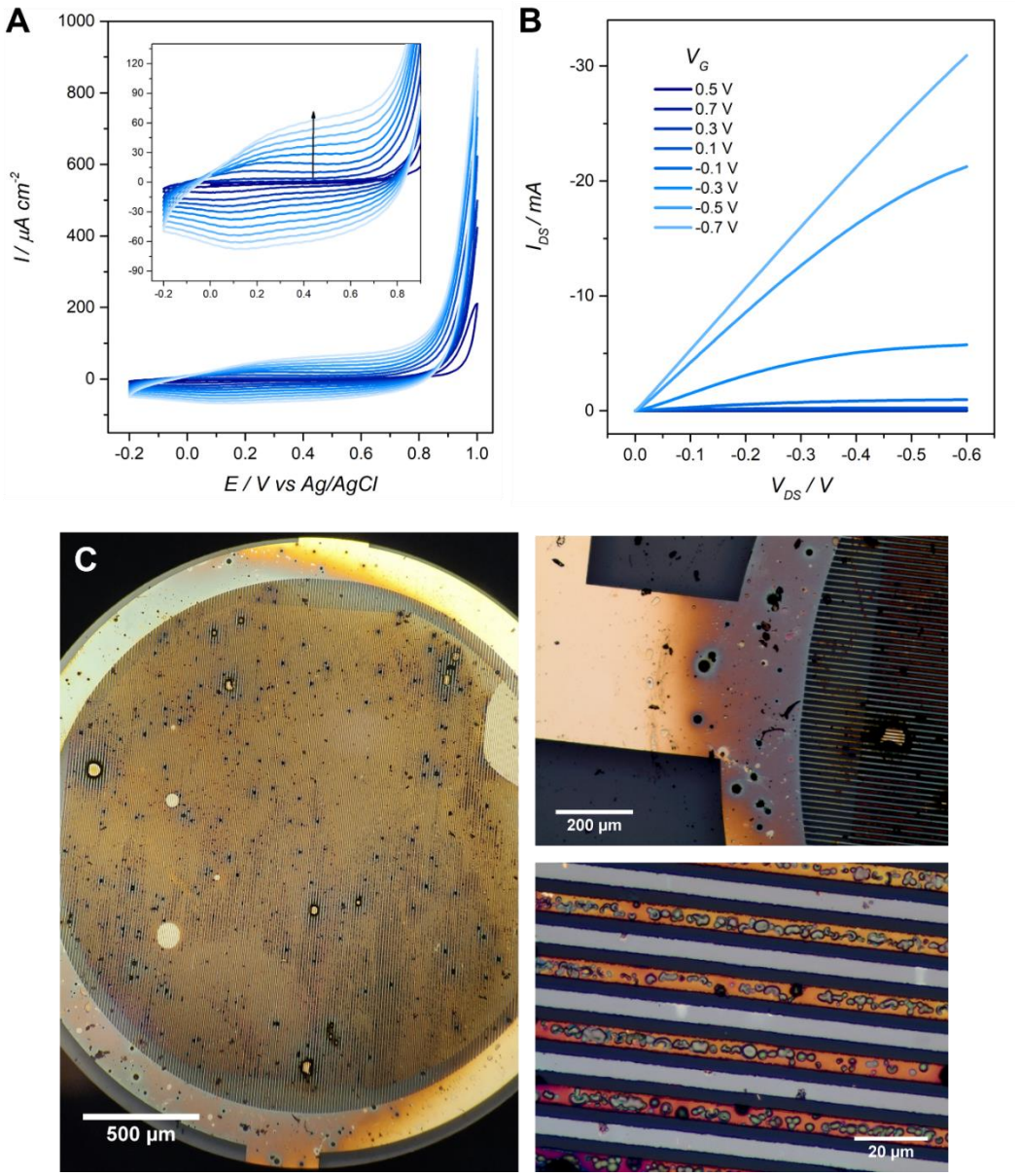

Figure S6. Voltammograms for the electropolymerization of PEDOT-N_3 on the IDEs ($HClO_4$ 0.1M, EDOT-N_3 10 mM, 40 mV/s, 10 cycles) **(A)**. Output curves for the obtained OECTs (1xPBS) **(B)**. Optical micrographs of the obtained OECTs at different magnifications **(C)**.

Electropolymerization in $HClO_4$ + SDS

The obtention of the devices was also performed in an acidic microemulsion solution ($HClO_4$ 0.1M, 10 mM EDOT, KCl 0.1 M, SDS 0.05M), according to a previously reported protocol.[4] From **Figure S7** it can be observed that the obtained films are more homogeneous than those obtained employing ACN or only $HClO_4$ as electrolyte. Moreover, the effect of the cycle number was studied, and transistors were obtained by performing 5, 10 or 20 electropolymerization cycles. As expected,[5] an increase in the cycle number (and therefore an increase in the thickness) yielded transistors with higher $V_{th}/V_{g,\ gm\ max}$.

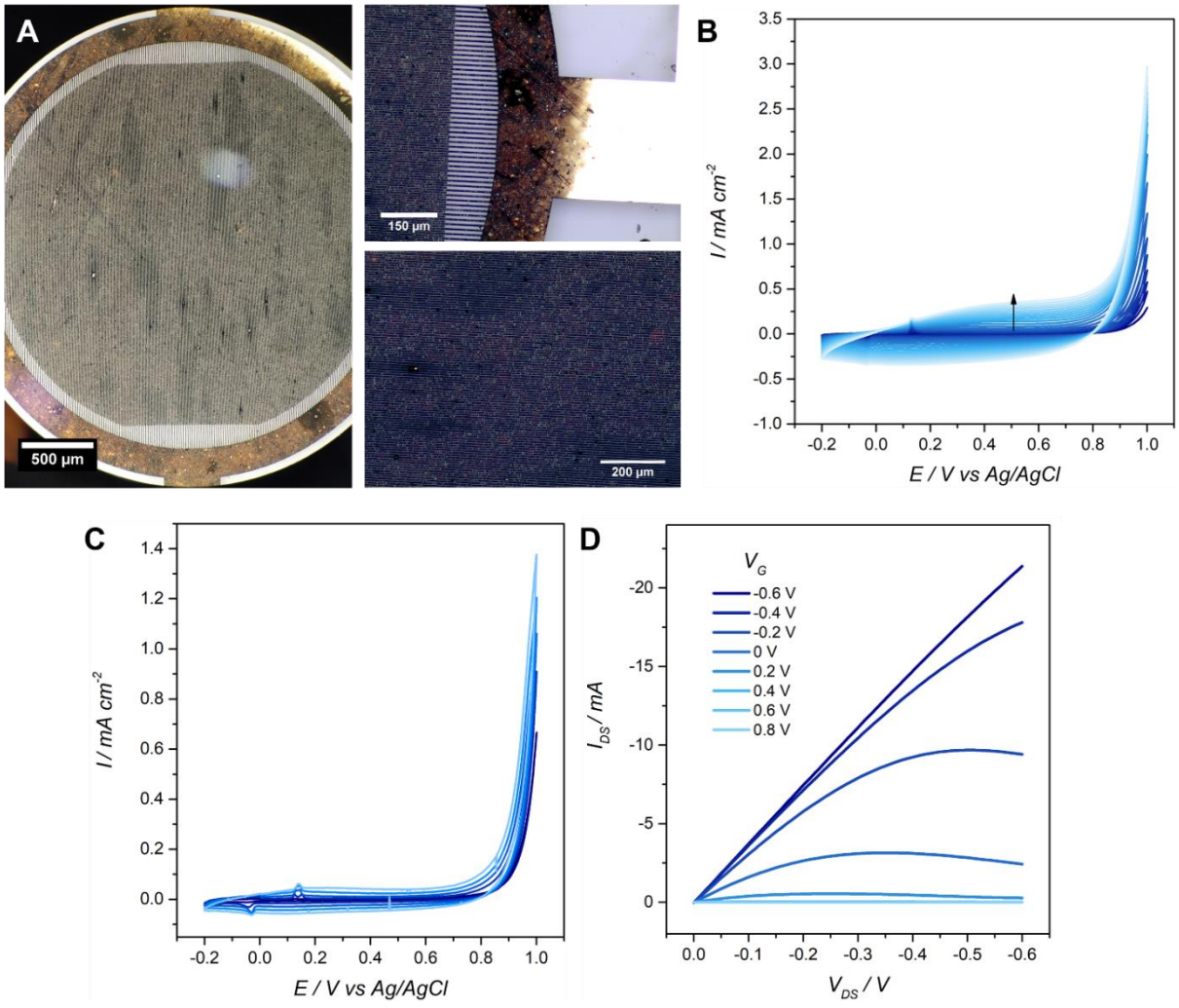

Figure S7. Optical micrographs of OECTs obtained from the $HClO_4$+SDS electrolyte employing 10 electropolymerization cycles at different magnifications **(A)**.Voltammograms for the electropolymerization of PEDOT-N_3 on the IDEs for 20 **(B)** and 5 **(C)** cycles ($HClO_4$ 0.1M, 10 mM EDOT-N_3, KCl 0.1 M, SDS 0.05M, 40 mV/s,). Output curves for the obtained OECTs for 5 cycles (1xPBS) **(D)**.

OECTs parameters computing

With the aim of benchmarking the electropolymerization protocols for the obtention of the PEDOT-N_3 OECTs, relevant parameters such as threshold voltage (V_{th}) and voltage of maximum transconductance ($V_{g,gm\,max}$) were computed. Firstly, V_{th} was extracted from the transfer characteristics curve plotted in the linear scale, as reported elsewhere.[6,7] The importance of extracting the V_{th} from the linear regime roots in the uniformity of the charge distribution along the channel observed under these conditions.[8] The maximum transconductance voltage was obtained from the first derivative of the transfer curve, as previously reported.[9]. **Figure S8** shows an example for the calculation of both parameters.

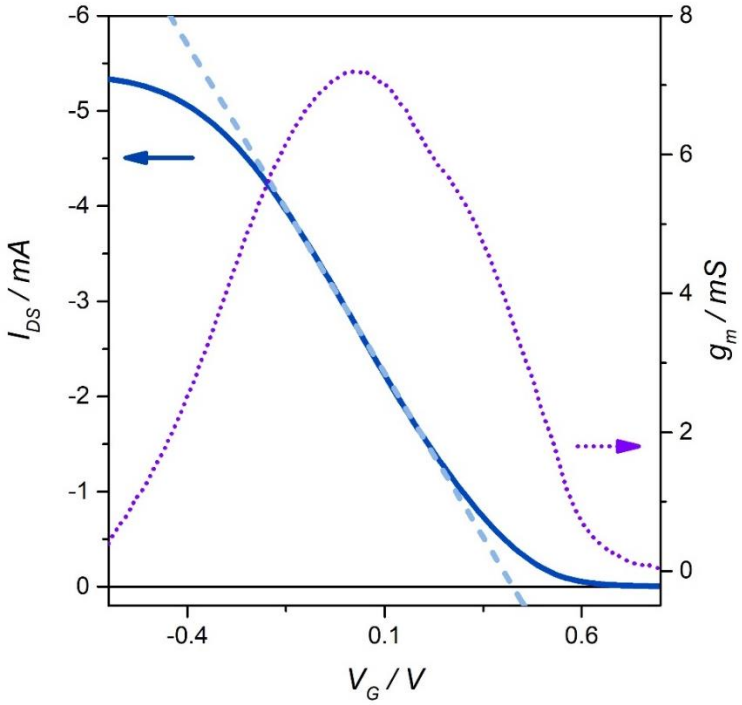

Figure S8. Transfer characteristics of a PEDOT-N_3 OECT obtained from a $HClO_4$-based electropolymerization and the corresponding first derivative (purple dots, right axis) of the transfer characteristics to obtain $V_{g,gm\,max}$. The linear fitting of the transfer characteristics performed to obtain the V_{th} values is shown as light blue dashed line (V_{DS} = -0.1V, 1xPBS)

Comparison of the obtention methods

In order to compare and benchmark the different OECTs obtained upon the different electropolymerization conditions, the maximum transconductance of the devices was plotted against either the threshold voltage or the maximum transconductance voltage. The maximum transconductance of the transistors it is known to be a main figure of merit of OECTs for the development of organic bioelectronic devices, showing the ability of the devices to amplify electronic signals and therefore to develop highly sensitive devices.[6,10] On the other hand, low threshold voltage and voltage of maximum transconductances are also preferred since a reduction in the V_{th} diminishes the power consumption and simplifies the circuit design by allowing the use of only one power supply.[5,11] More important, the operation of the transistors at V_G = 0 V prevents the alteration of anchored bio-entities, such as proteins, lipid bilayers or cells, which could degrade at high applied voltages.[12] Similarly, the recognition processes are less affected by the application of very low electrical fields.[13]

From **Figure S9** and **Figure S10** it is observed that the devices obtained from ACN show high transconductance values but also very high $V_{th}/V_{gm,max}$. When an aqueous electrolyte such as $HClO_4$ is employed, the obtained OECTs show lower g_m and $V_{th}/V_{gm,max}$. Interestingly, the addition of SDS and KCl to the acidic electrolyte increases the g_m while keeping low $V_{th}/V_{gm,max}$ values. This result can be ascribed to the creation of new paths for ionic transport by the surfactant.[4,6] Finally, best trade-off is observed when employing 10 electropolymerization cycles in the acidic microemulsion electrolyte, giving OECTs with low $V_{th}/V_{gm,max}$ while keeping relatively high $g_{m,max}$ values.

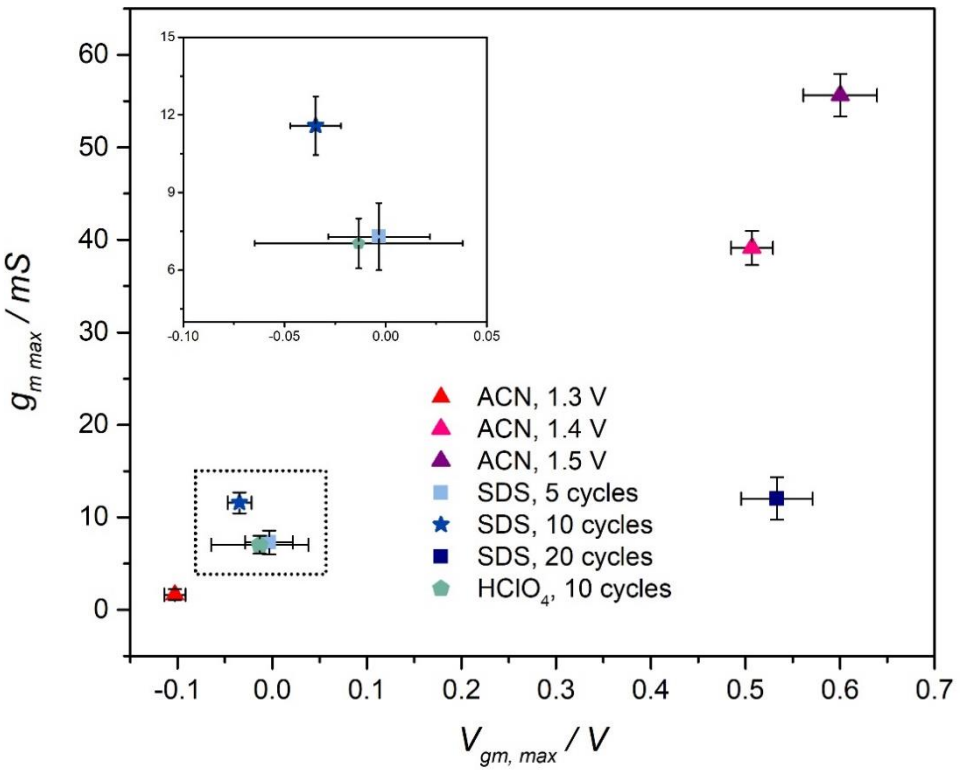

Figure S9. OECTs comparison obtained upon the different electropolymerization conditions.

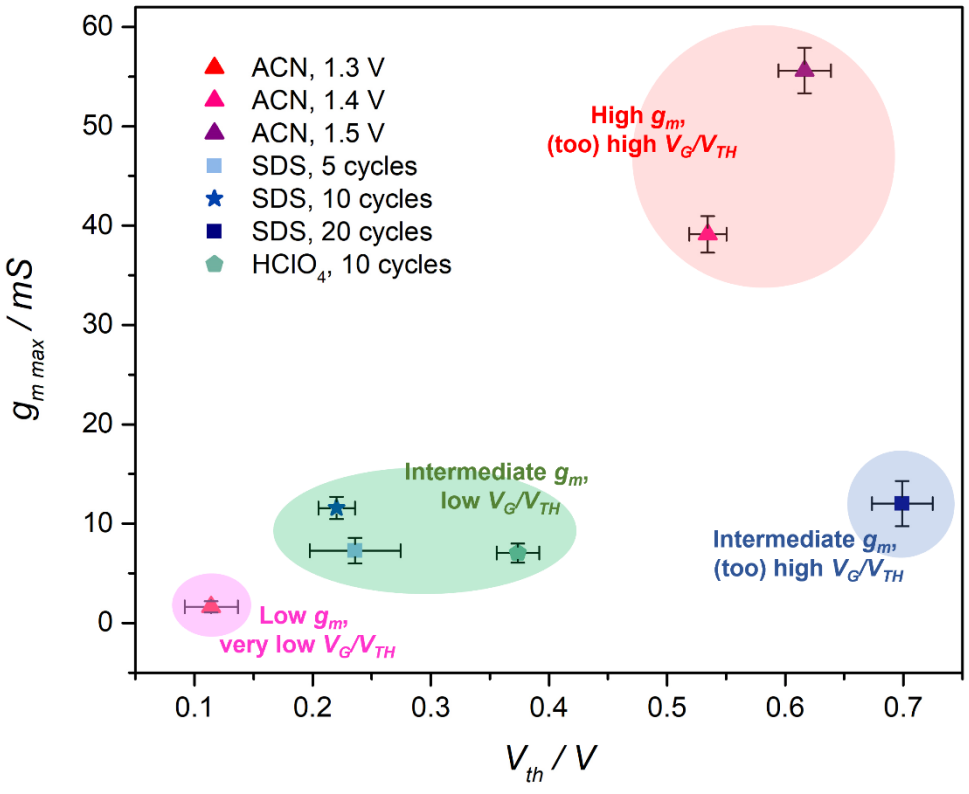

Figure S10. OECTs comparison obtained upon different electropolymerization conditions.

Reproducibility of the SDS-based obtention protocol

In order to study the reproducibility of the chosen protocol, the resistance of 17 different devices was analyzed and shown in a box plot (**Figure S11**). It can be observed that the RSD is lower than 15% for the obtained transistors, accounting for a great reproducibility of the obtention method.

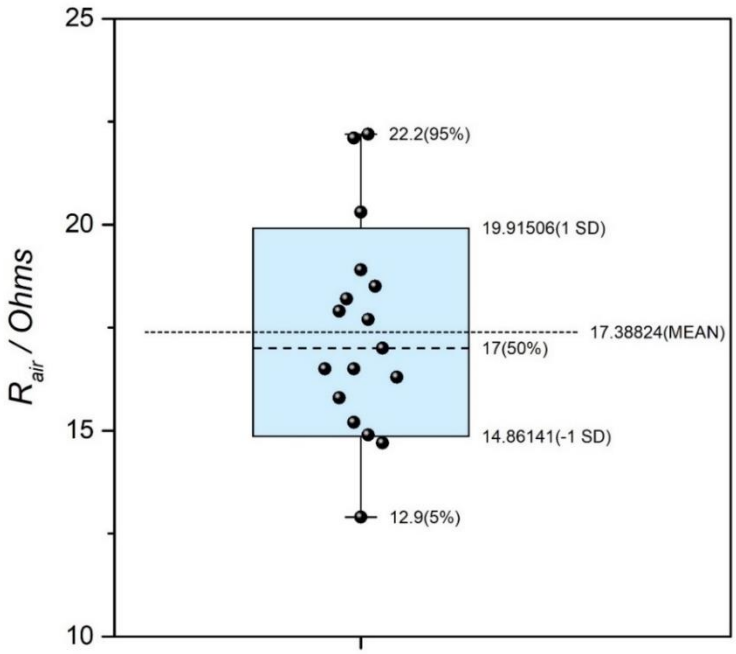

Figure S11. Box plot for the resistance between drain and source electrodes measured after synthesis in dry state of 17 different PEDOT-N_3 OECTs obtained by electropolymerization in SDS+$HClO_4$.

PEDOT and PEDOT-N_3 comparison

In order to compare the performance of the PEDOT-N_3 transistors with that of PEDOT-based OECTs, PEDOT without azide moieties was electropolymerized on IDEs employing the same protocol as the one chosen for the PEDOT-N_3 OECTs (**Figure S12(A)**). Similar current densities can be observed for the electropolymerization curves of both monomers, indicating comparable thickness of the polymer channel, and allowing the comparison of both transistors. The $V_{G,\ gm\ max}$ was calculated and plotted in **Figure S12(B)**. It is observed that PEDOT-N_3 OECTs show lower $V_{G,\ gm\ max}$ values than PEDOT OECTs. In addition, $V_{G,\ gm\ max}$ is very close to 0 V for PEDOT-N_3 OECTs which, as it was previously stated, is a highly advantageous feature of these transistors.

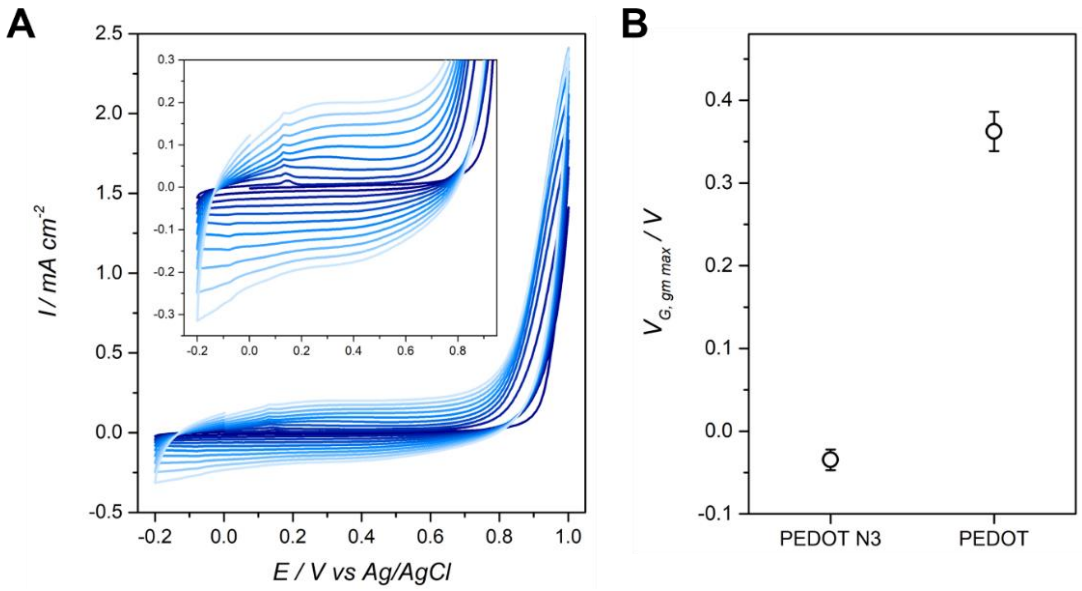

Figure S12. Electropolymerization curves for a PEDOT-OECT ($HClO_4$ 0.1M, 10 mM EDOT, KCl 0.1 M, SDS 0.05M, 40 mV/s, 10 cycles) **(A)**.Comparison of $V_{G,\ gm\ max}$ for PEDOT and PEDOT-N_3 OECTs **(B)**.

The resistance measured (in air) between both source and drain electrodes after the electropolymerization was 17.4 Ω for PEDOT-N_3 OECTs and 14.9 Ω for PEDOT OECTs. Next, while the difference in the structure of the monomers has been reported to significantly affect the conductivity of the obtained polymers, showing that the PEDOT-N_3 polymer is less conducting that PEDOT,[14] the difference in the obtained resistance after the electropolymerization was not as big as it could have been expected. In addition, similar results are observed for the transfer characteristics of the OECTs, where the ON I_{DS} values for both PEDOT and PEDOT-N_3 transistors are in the range of 5-6 mA (at the same V_{DS}). Next, we hypothesize that the use of the IDEs allows for the channel to overcome the lower conductivity of the PEDOT-N_3, resulting in efficient transistors with performances comparable to those of PEDOT-based OECTs.

PEDOT-N_3-OECTs characterization

Transient measurements

The ON switching of the PEDOT-N_3 devices was also evaluated by performing the repeated cycling of the OECTs between 0 V and the ON state while recording the drain-source current at a constant V_{DS} (**Figure S13**). Next, the obtained source-drain current response was adjusted to an exponential decay to obtain t_{on} and t_{off} for each set of transistors, as previously described.[6,15,16]

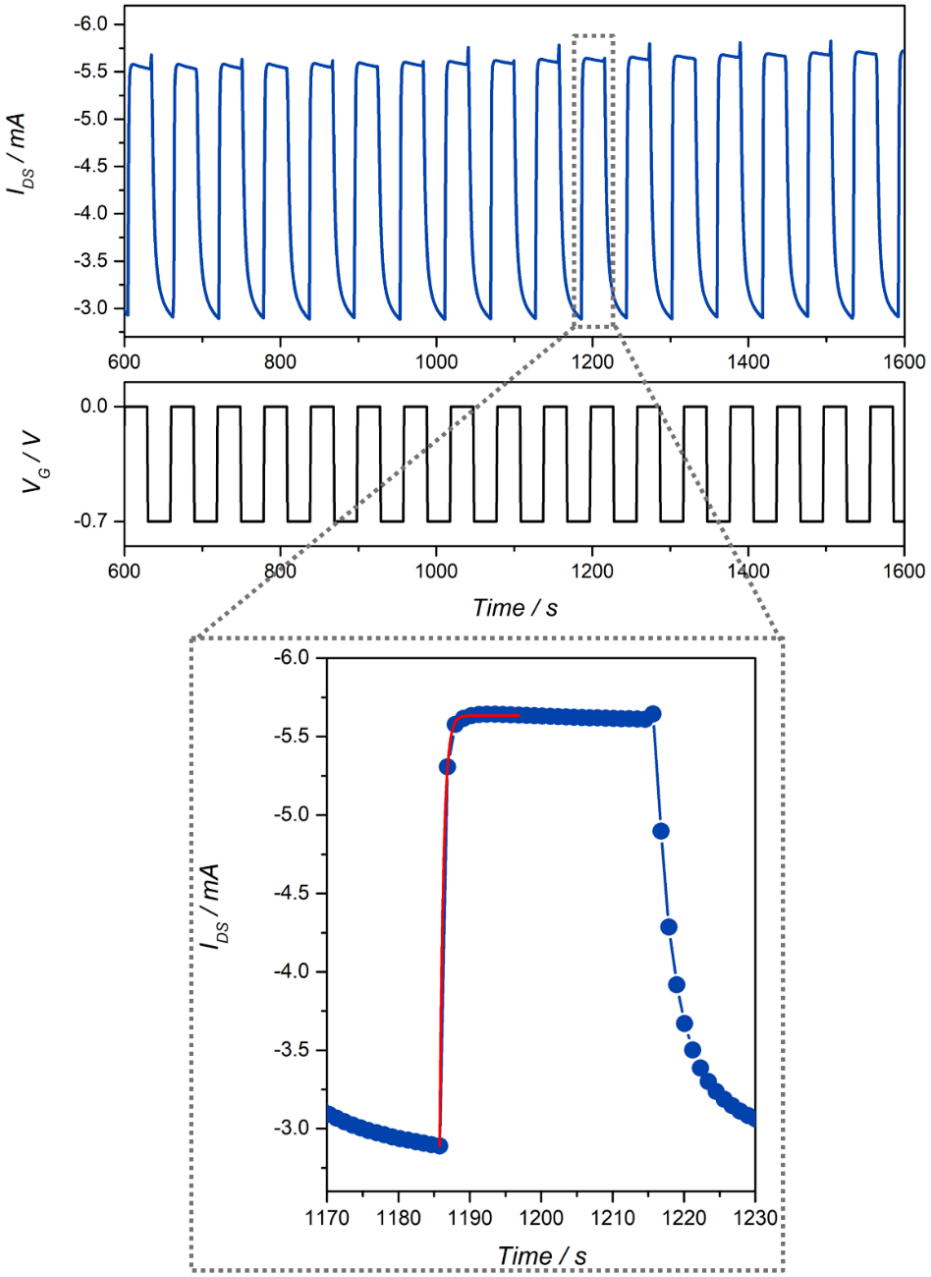

Figure S13. Transient characteristics (ON switching) of a PEDOT-N_3 OECT (up) and example of the fitting to obtain the t_{on} and t_{off} values (down) (V_{DS} = -0.1 V, 1xPBS)

EIS measurements

Electrochemical Impedance Spectroscopy (EIS) measurements were performed in order to obtain more information about the electrical features of the PEDOT-N_3 films deposited onto the IDEs. The spectra were obtained at different potentials and the Nyquist plots are shown in **Figure S14(A)**. Moreover, the spectra were fitted to the circuit shown in **Figure S14(A)**. The circuit was based in previously reported EIS measurements of PEDOT-based OECTs,[17,18] and consisted of a solution resistance (Rs) connected in series to two parallel branches containing, in one side, a CPE, and in the other branch a series connection of the electronic/charge transfer resistance and a double layer capacitance. The CPE element accounts for the porous interface between the polymer domains and the inner solution interface, showing the typical "capacitance dispersion" and therefore a deviation from the ideal capacitive element.[19] The R_E resistance is ascribed to the charge transport process along the conducting polymer domains, while the C_{DL} accounts for the capacitance of the electrode-solution interface of the gold contacts. The results for the fitting are shown in **Table S1**.

It is worth noting that for the fitting of the spectrum obtained at -0.5 V, a Warburg O element was added, which is suitable for studies involving diffusing species when the DC current is different than zero, i.e., away from the OC potential, where the current would decay in time.[20,21] This is the particular situation of the biased electrode here reported, which at this potential undercomes reduction, as shown in the change of R_E in main text, **Figure 3**. This element has been previously utilized in several works involving the fitting of PEDOT-based electrodes impedance spectra.[20,22] Furthermore, the capacitance was calculated according to $C = 1/(2\pi f(Im(Z))$ [23] and it is shown in **Figure S14(B)**. The small differences observed in R_S can be ascribed to the conducting polymer film resistance in its non-conducting state, which can also contribute to this high frequency resistance, as previously reported.[19]

Table S1. Results for the fitting of the EIS spectra.

E [V]	R_S [Ω]	Error R_S [Ω]	R_E [Ω]	Error R_E [Ω]	C [F]	Error C [F]	$Y_{0,CPE}$ [S.s^n]	n_{CPE}
-0.8	143.2	3.4	61905	2197.6	2.5E-06	6E-08	-	-
-0.5	136.9	1.6	40378	1888.9	-	-	5E-06	0.8
-0.2	125.8	1.4	453.5	21.3	6.7E-06	2E-07	5E-05	0.6
0.1	111.2	2.7	38.9	5.8	6.0E-06	3E-07	5E-05	0.5
0.4	125.8	1.4	14.7	0.3	5.3E-06	2E-07	9E-05	0.5
0.7	124.7	1.1	13.5	0.3	4.0E-06	2E-07	1E-04	0.5

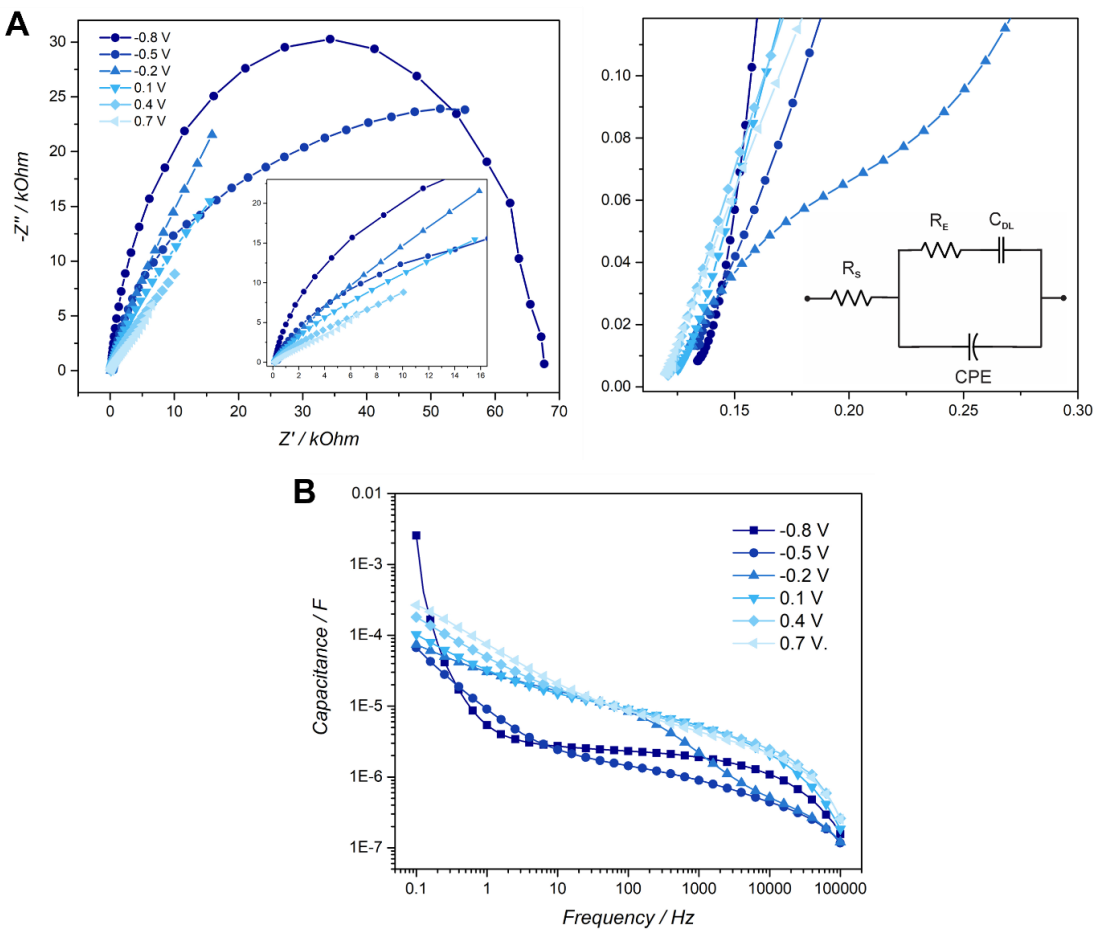

Figure S14. Nyquist plot of the impedimetric response of the PEDOT-N_3 electrode (left) and zoom together with the circuit employed to fit the spectra (right) **(A)**. Capacitance obtained from the EIS spectra **(B)**.

AFM measurements

The morphology of the channel area of the fabricated OECTs was investigated by AFM measurements (**Figure S15**). Smooth films are observed, showing a RMS of 1 nm, in close agreement with previously reported results.[4]

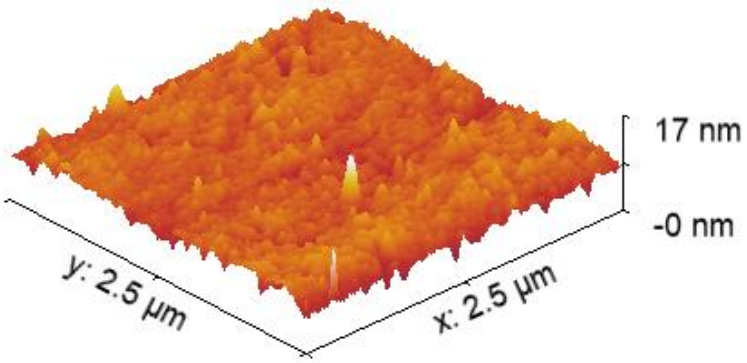

Figure S15. AFM topography image of the channel area of a PEDOT-N_3 OECT.

ATR-FTIR measurements

To corroborate the presence of the azide moieties after the electropolymerization protocol, ATR-FTIR measurements of the OECTs were performed. From **Figure S16** it is observed that the spectrum of the PEDOT-N_3 film (obtained from the SDS-$HClO_4$ solution) shows the typical azide band at ca. 2100 cm^{-1}, in agreement with previously reported studies.[2] Further description of the FTIR spectrum of the fabricated OECTs is presented in **Table S2**. The spectrum shows the presence of PEDOT-N_3 bands as well as SDS ones, corroborating the incorporation of the SDS anions into the polymer film during the polymer electrosynthesis.

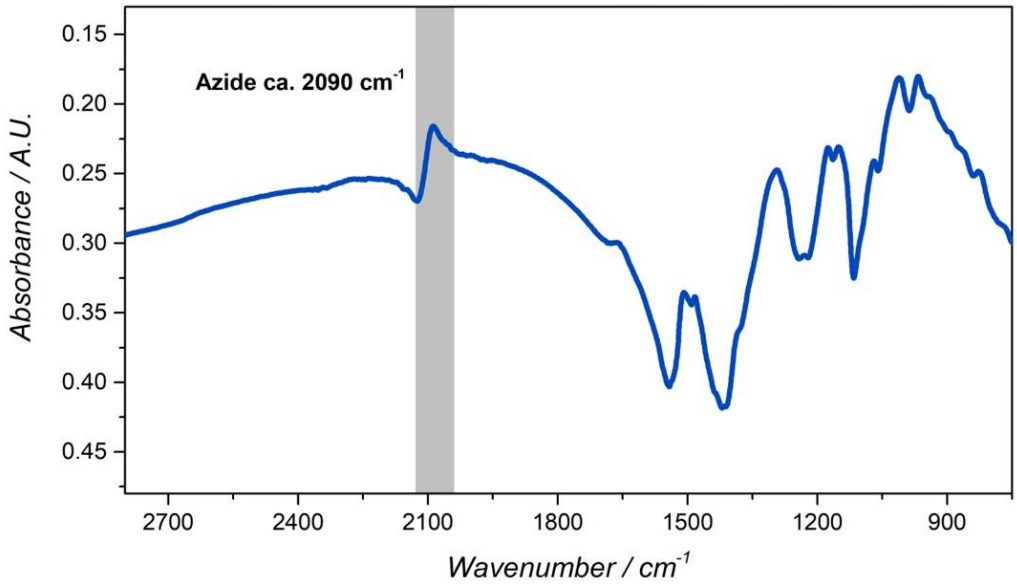

Figure S16. ATR-FTIR spectrum of a PEDOT-N_3 OECT.

Table S2. FTIR bands assignment.

Wavenumber	Assignment	References
2090 cm^{-1}	Azide asymmetric stretching	2,24
1509 cm^{-1}	Asymmetric C=C stretching	25,26
1483 cm^{-1}	Deformations of CH_2 and CH_3	27
1294 cm^{-1}	Aromatic C-O stretching	26
1175 cm^{-1}	Asymmetric stretching of SO_3^-	28,29
1151 cm^{-1}	Asymmetric stretching of SO_3^-	28,29
1070 cm^{-1}	Symmetric S-O stretching	30
1010 cm^{-1}	In-plane aromatic C-H bending	25,28,29
967 cm^{-1}	Symmetric S-O stretching	30

Click of redox probes and control experiments

In order to perform a control experiment of the clicking of the ethymyl-ferrocene redox probe on the transistors, PEDOT (without azide moieties) was electropolymerized on IDEs through the same protocol as the one employed for the PEDOT-N_3 OECTs. Next, the electrode was exposed to the same clicking process as the PEDOT-N_3 one, and the electrochemical and electrical features were obtained (**Figure S17**). As described in the main text, no significant differences are observed after the treatment with Et-Fc, accounting for the specificity of the click reaction on the azide-modified OECTs/electrodes.

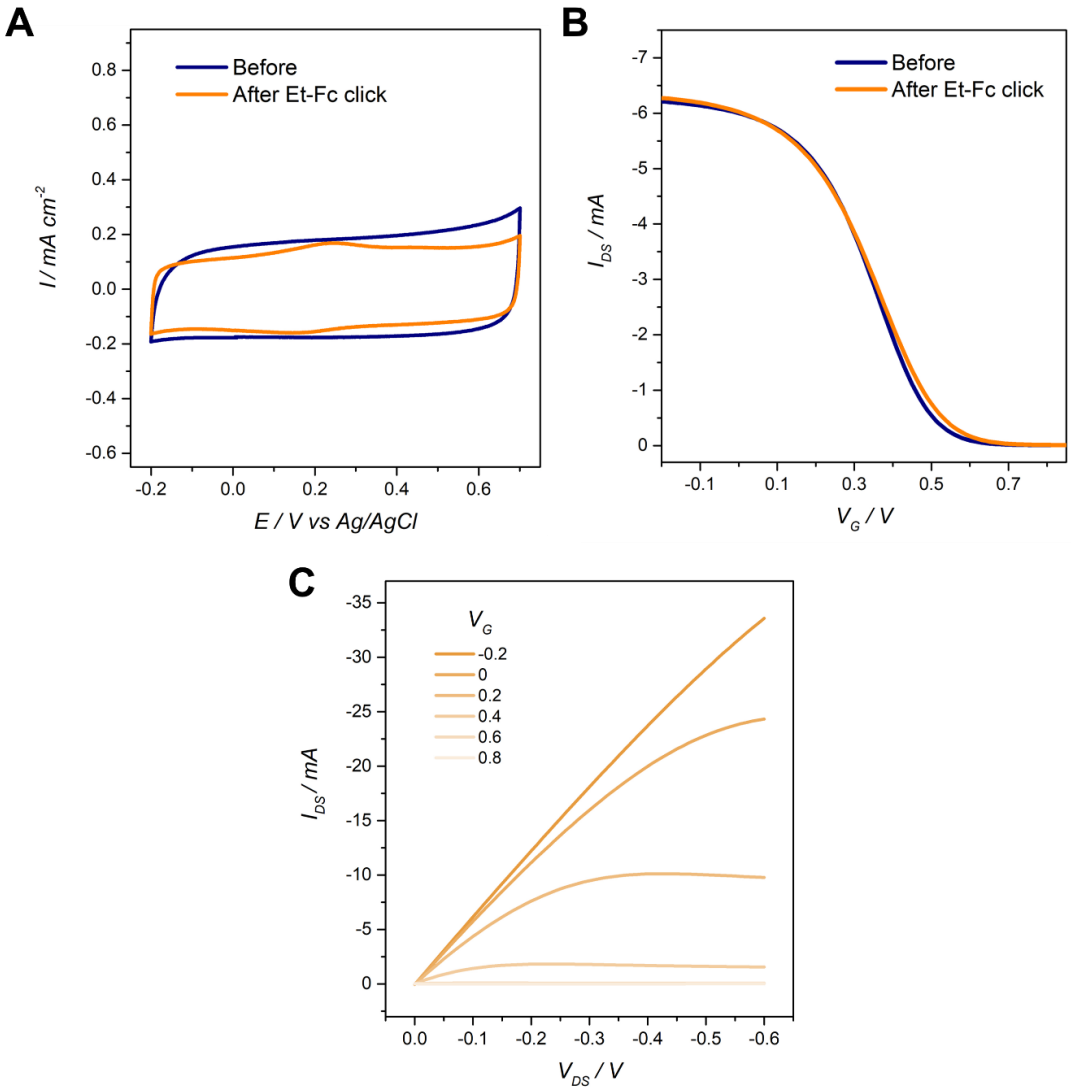

Figure S17. Cyclic voltammetry curves for a PEDOT electrode before and after the click reaction with Et-Fc (50 mV/s, 1xPBS) **(A)**. Threshold voltage and maximum transconductance for a PEDOT OECT before and after the click reaction with Et-Fc **(B)**. Output characteristics for a PEDOT OECT after the click reaction with Et-Fc **(C)**.

Figure S18 shows the output characteristics of the PEDOT-N_3 OECTs after the click reaction with Et-Fc, proving that the transistors keep their performance after the click functionalization.

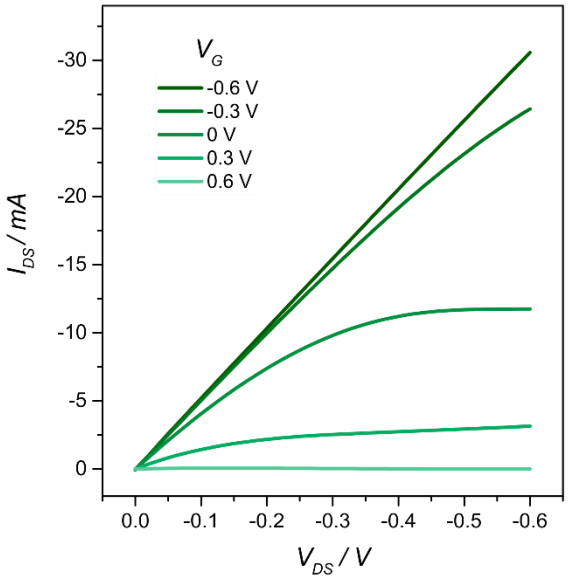

Figure S18. Output characteristics of the Et-Fc clicked PEDOT-N_3 OECTs (1xPBS).

Regarding the clicking of the N-But redox probe, chronoamperometry measurements were employed to perform the clicking of the redox probe. **Figure S19** shows an example of the chronoamperometry curves obtained. Moreover, the voltammograms of the PEDOT-N_3 electrode before and after the "electro"clicking process are shown in **Figure S20**, confirming the effective clicking of the redox probe. In addition, it is observed that the transistors conserve their features after the clicking process and the electrochemistry measurements in the organic solvent, proving great stability (**Figure S21**).

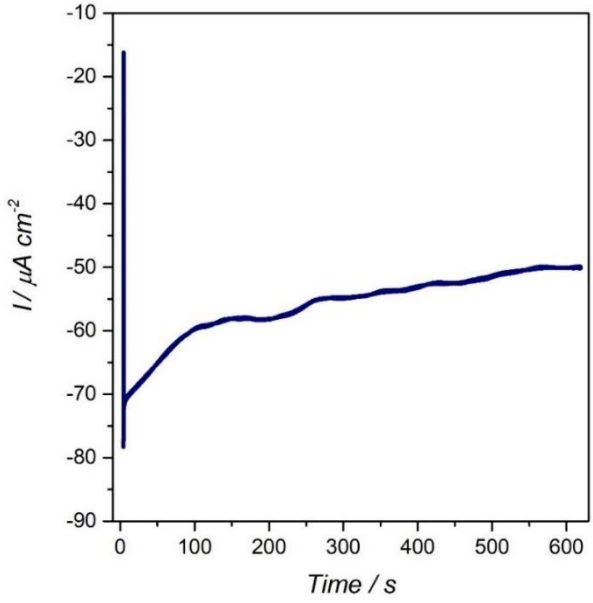

Figure S19. Chronoamperometry measurements for the "electro"clicking of N-But on PEDOT-N_3 electrodes (-0.75 V, 10 mM N-But, 2 mM $CuSO_4.5H_2O$, DMF).

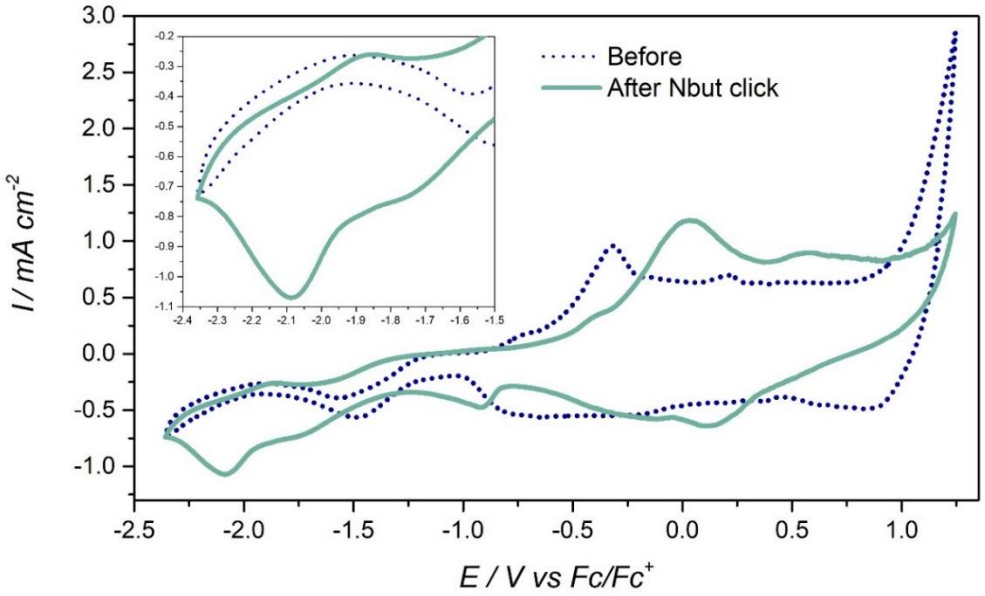

Figure S20. Cyclic voltammetry curves of the PEDOT-N_3 electrode before and after the "electro"clicking of N-But process ($TBAF_6$ 0.1M, ACN, 50 mV/s).

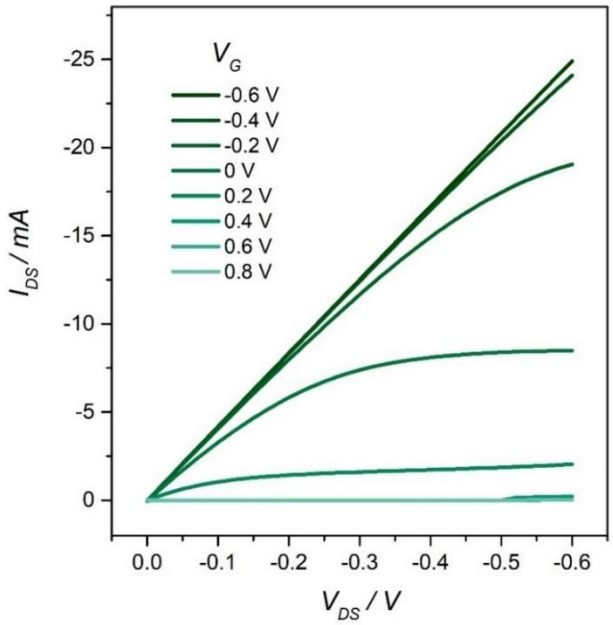

Figure S21. Output characteristics of the N-But clicked PEDOT-N_3 OECTs (1xPBS).

FO-SPR measurements

The electropolymerization of the PEDOT-N_3 film on the FO was performed following the chosen SDS-$HClO_4$-based protocol. To this end, the FO probes were connected to the potentiostat as WE by means of a copper tape, and the electropolymerization area was delimited by a liquid heat shrink tubing, as previously described (**Figure S22(A)**).[1] In this case, only 5 electropolymerization cycles were employed in order to obtain a thinner polymer film and therefore not overcome the SPR probing depth. A typical electropolymerization curve is observed in **Figure S22(B)**. From such curves an average PEDOT-N_3 film thickness on the fiber of 68 ± 5 nm was derived. It is observed that the current densities values are similar to those observed for the OECTs (when 5 cycles were employed), validating the comparison between the FO-SPR experiments and those employing the transistors as platform.

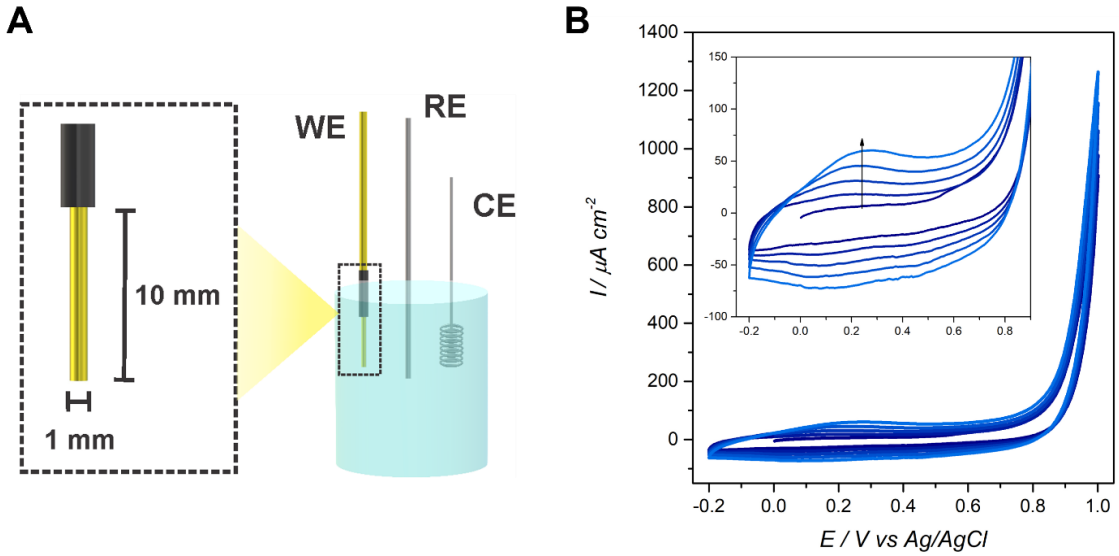

Figure S22. Setup for the electropolymerization of PEDOT-N_3 (and PEDOT) on the FO **(A)**. Electropolymerization curves for a FO (($HClO_4$ 0.1M, 10 mM EDOT-N_3, KCl 0.1 M, SDS 0.05M, 40 mV/s, 5 cycles) **(B)**.

Next, after the electropolymerization of PEDOT-N_3 on the FO, a resonance dip can be observed in the reflected spectra measured in air due to the polymer film attached to the fiber surface. (**Figure S23(A)**). A picture of the Au-polymer edge is shown in **Figure S23(B)**.

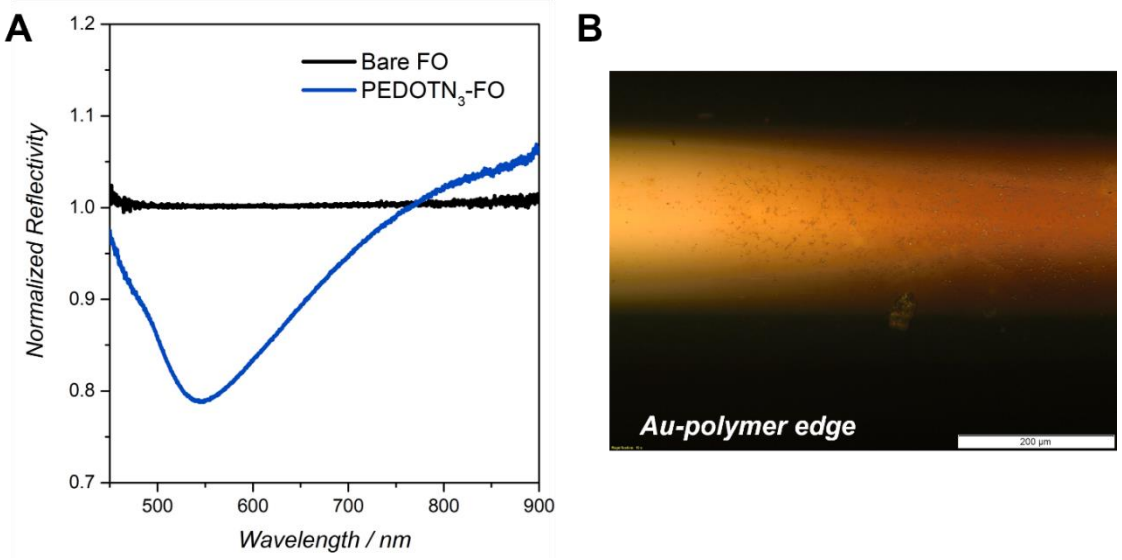

Figure S23. Spectra of a FO in air before and after electropolymerization of PEDOT-N_3 layer **(A)**. Optical microscope image of a PEDOT-N_3 modified fiber after the electropolymerization process at the Au-polymer edge **(B)**.

Next, in order to perform the clicking of the acetylene-PEG_4-biotin molecules, the PEDOT-N_3-modified FO was dipped in the DMSO-based solution containing the alkyne, as described in the Materials and Methods section. The FO was subsequently rinsed with DMSO, KCl 3M and Milli-Q water. In addition, and with the aim of taking the polymer back to its conducting state after the clicking procedure and thus recover the optical signal, a few cyclic voltammetry curves were performed in 1xPBS after the click reaction and the FO-PEDOT-N_3 was left at its conducting state (**Figure S24(A)**). The spectra in air of the PEDOT-N_3-FO before and after the acetylene-PEG_4-biotin clicking procedure are shown in **Figure S24(B)**.

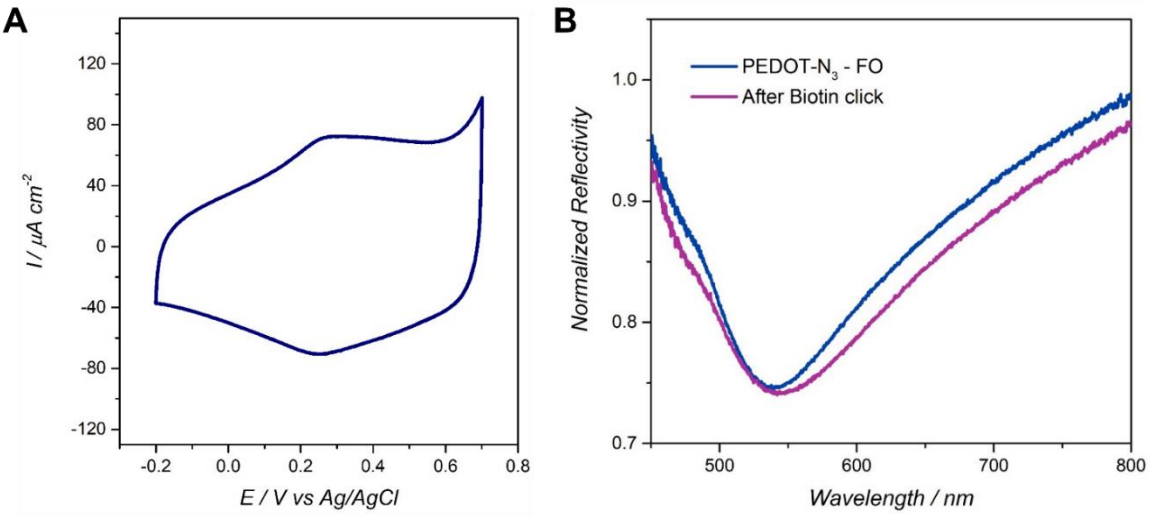

Figure S24. Cyclic voltammetry curves for a biotin-PEDOT-N_3-FO in 1xPBS after the clicking procedure (1xPBS, 50 mV/s). **(A)**. Air spectra of a PEDOT-N_3-modified FO before and after click reaction with acetylene-PEG_4-biotin **(B)**.

The shifts in the resonance wavelength were analyzed by fitting the to a second-order polynomial, as shown in **Figure S25**. For the shift obtained for the Biotin-PEG_4 clicking.

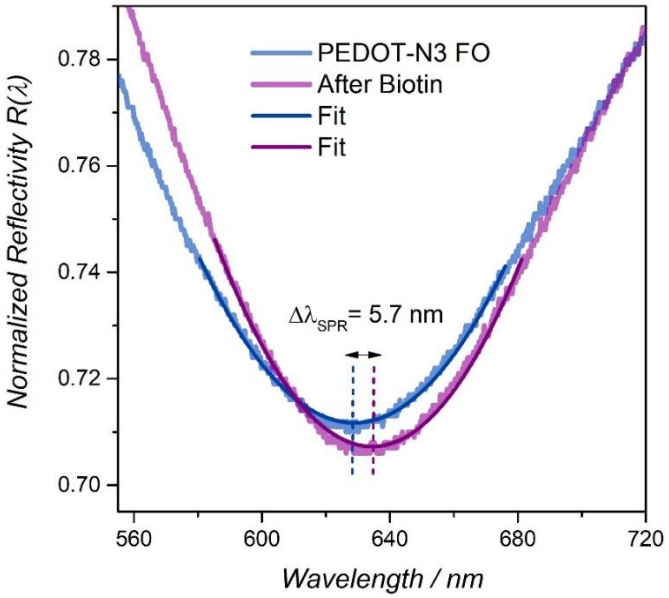

Figure S25. FO SPR spectra of a fiber in Milli-Q after PEDOT-N_3 electropolymerization and click of the acetylene-PEG_4-biotin with their corresponding fittings to a second-order polynomial.

In order to further analyze the measured spectral shifts upon FO surface modification, the obtained results were correlated with Fresnel reflectivity-based simulations implemented in custom made Maple V scripts. The curved surface of the optical fiber was approximated by a stack of planar layers with dispersive refractive index. The thickness of the added surface layers was fixed: for the PEDOT-N_3 film, the employed value was obtained from the CV measurements, while for the different bio-layers (such as biotin, neutravidin, HD22 and thrombin) the thickness utilized was based on published dimensions of the respective compounds. Spectra for different refractive indices were simulated and the resonance wavelength of those spectra was determined *via* second order polynomial fit, as shown in **Figure S26(A)** and (**C)**, for the PEDOT-N_3 film and the NeutrAvidin layer, respectively. A linear calibration curve was constructed based on the simulated spectral shifts and used to correlate the measured spectral shifts to the respective refractive index of the added surface layer (**Figure S26(B)** and **(D)**). Refractive indexes of 1.372 and 1.45 were obtained for PEDOT-N_3 and NeutrAvidin, respectively. Obtained results were in good agreement with previously reported values for PEDOT films[31] and adsorbed protein layers,[32] validating the employed approach for signal analysis.

The surface mass density was calculated based on obtained values for refractive index and thickness of the surface layers using the equation[33]

$$\Gamma = d_p \cdot (n_p - n_s) \cdot \left(\frac{\partial n}{\partial c}\right)^{-1} \qquad \textbf{Equation S1}$$

Where n_p and n_s are the refractive indices of polymer/protein layer and an aqueous media (n_s = 1.333), respectively, and d_p corresponds to the polymer/protein layer thickness. The factor $\partial n/\partial c$ relates the changes in refractive index with the concentration of (bio)molecules bound to the surface and was set to 0.2 mm^3/mg.[34]

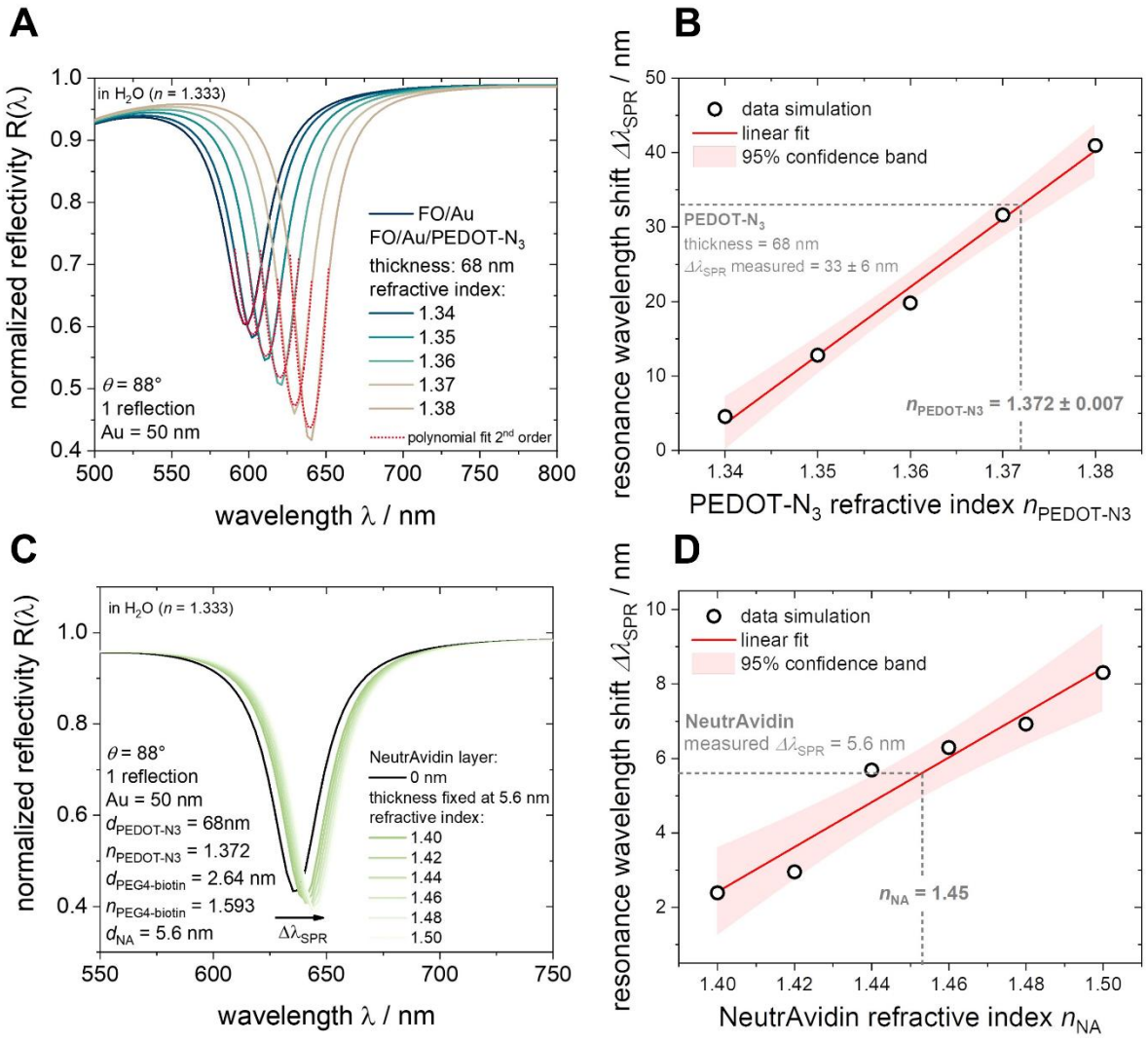

Figure S26. Simulated spectra obtained for FO probes coated with a PEDOT-N$_3$ film (d_p = 68 nm) and refractive index variation **(A)**. Linear calibration curve for the PEDOT-N$_3$ refractive index **(B)**. Simulated spectra for various refractive indices associated with a NeutrAvidin layer (d_p = 5.6 nm) immobilization on FO probes coated with PEDOT-N$_3$ after biotin click reaction **(C)**. Linear calibration curve for the NeutrAvidin refractive index **(D)**.

In order to perform a control experiment for the clicking of the biotin molecules, PEDOT (without azide moieties) was electropolymerized on the FO following the same protocol as for PEDOT-N$_3$. Next, the PEDOT-FO was subjected to the same clicking protocol employing the acetylene-biotin molecule in DMSO. **Figure S27(A)** shows the electropolymerization curves of PEDOT on a FO and **Figure S27(B)** shows optical microscope images of the modified fiber, clearly displaying the

deposition of the polymer film. The spectra of the FO before and after the polymer deposition, and after the clicking reaction are shown in **Figure S27(C)**. No significant change is observed in the reflectivity minimum of the polymer-modified fiber after exposing it to the biotin click reaction conditions, as expected for the azide-free PEDOT employed.

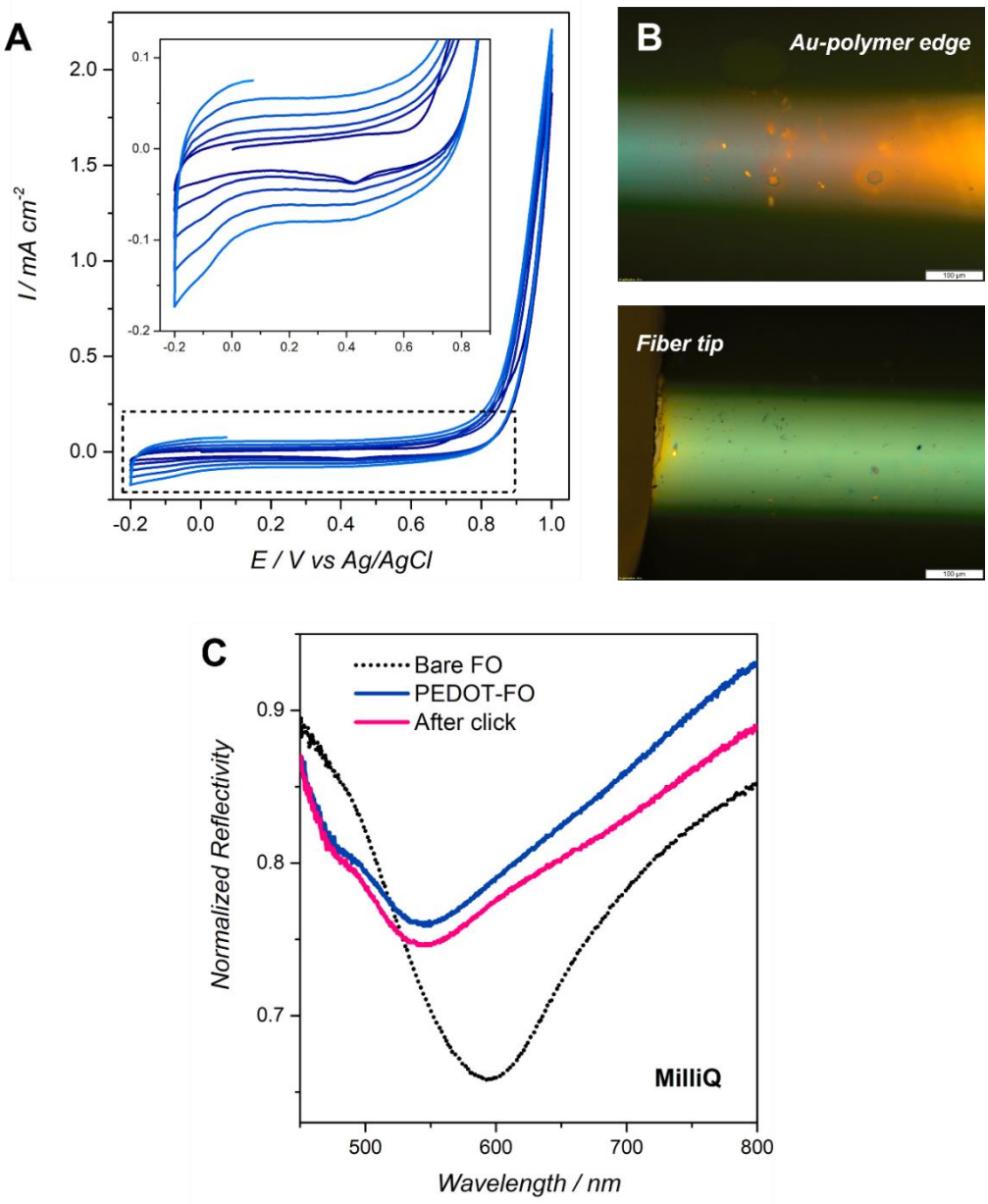

Figure S27. Electropolymerization curves for a FO (($HClO_4$ 0.1M, 10 mM EDOT, KCl 0.1 M, SDS 0.05M, 40 mV/s, 5 cycles) **(A)**. Optical microscope images of a PEDOT-FO **(B)**. Milli-Q spectra of a FO before and after PEDOT electropolymerization and after click reaction with acetylene-PEG_4-biotin **(C)**.

Similarly to what was performed for PEDOT-N_3-FO, a few cyclic voltammetry curves were performed in 1xPBS after the exposition of the PEDOT-FO to the click reaction conditions, leaving the polymer modified FO at its conducting state (**Figure S28(A)**). The effect of the potential cycling on the SPR

response of the PEDOT-FO is clearly observed in **Figure S28(B)**. These potential-dependent changes of the SPR signal are in agreement with previously reported findings and can be associated to the electrochromic behavior of the PEDOT film, showing significant changes of the resonance wavelength when going from the doped state to the de-doped state of the film.[31] A similar electrochromic behavior was observed for the PEDOT-N_3 film as described above.

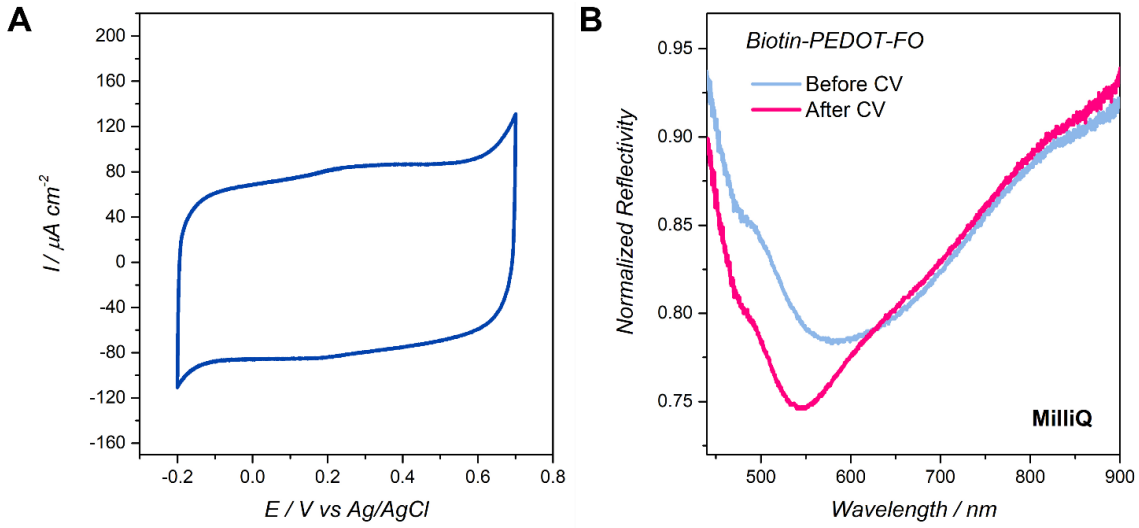

Figure S28. Cyclic voltammetry curves for a PEDOT-FO in 1xPBS after the biotin clicking procedure (1xPBS, 50 mV/s) **(A)**. Spectra of a biotin-PEDOT-FO before and after CV measurements in Milli-Q **(B)**.

Clicking of biotin and avidin recognition on OECTs

The same clicking and recognition protocol employed for the FO was used in order to incorporate biotin moieties and NeutrAvidin to the surface of PEDOT-N_3 OECTs. From **Figure S29** it is observed that the transistors conserve their features after the clicking process in the organic solvent and the NeutrAvidin recognition, showing great stability.

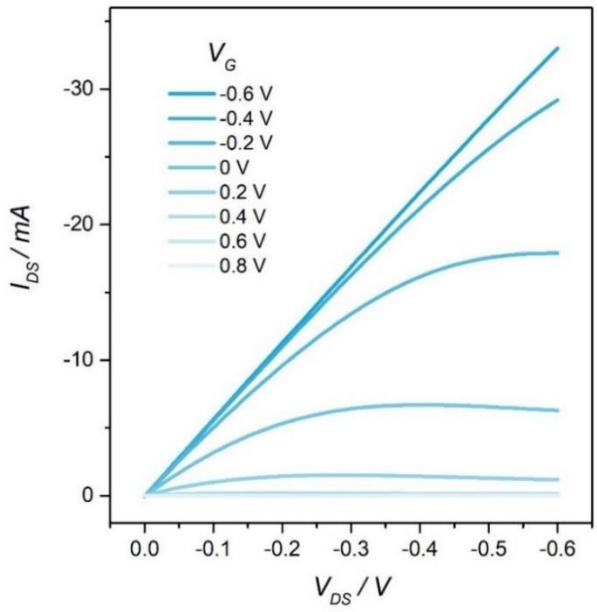

Figure S29. Output characteristics of a NeutrAvidin-biotin-PEDOT-N_3 OECT (1xPBS).

On the other hand, biotin-PEDOT-N_3 OECTs were also employed in order to anchor streptavidin-HRP conjugate, making use of the biotin-avidin biorecognition. **Figure S30** shows the transfer characteristics of the HRP-biotin-PEDOT-N_3 OECT together with the calculated transconductance. It is observed that the OECTs present a $V_{G,\ gm\ max}$ close to 0 V, endowing the application of 0 V while preserving an optimal g_m value.

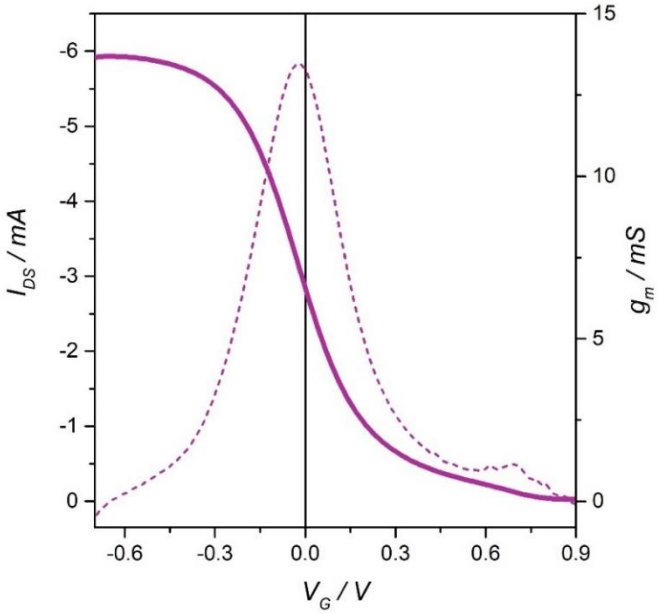

Figure S30. Transfer characteristics and transconductance of an HRP-biotin-PEDOT-N_3 OECT (V_{DS} = -0.1 V, 1xPBS).

Thrombin sensing experiments

To check the specificity of the response of the HD22-modified PEDOT-N_3 OECTs, the same modification protocol was performed on PEDOT OECTs, without azide moieties, and their response towards thrombin was evaluated (**Figure S31**). As described in the main text, the transistors did not show a response towards the cardiac biomarker, probing the specific recognition of thrombin by the HD22 clicked devices. In addition, the same experiment was performed by PEDOT-modified FO setup (main text).

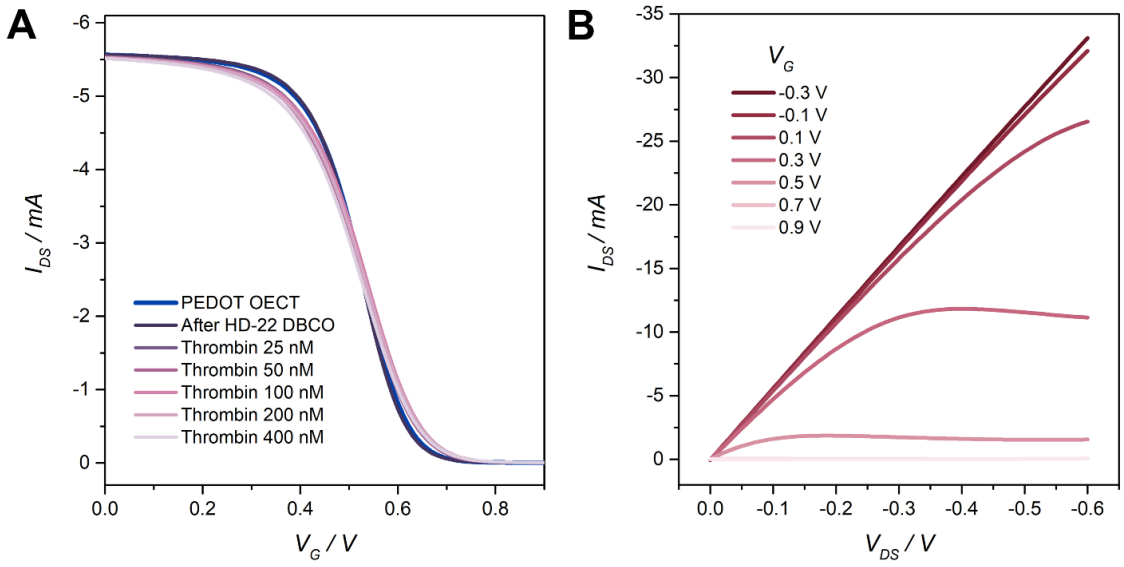

Figure S31. Transfer characteristics curves of a PEDOT OECT before and after DBCO-HD22 functionalization and further thrombin recognition (V_{DS} = -0.1V, 1xPBS) (**A**). Output characteristics of a PEDOT-HD22 OECT after treatment with 400 nM thrombin **(B)**.

Moreover, the PEDOT-N_3-HD22 OECTs employed for thrombin sensing showed no alteration of the output characteristics after the modification and recognition process, proving the excellent stability of the developed transistors (**Figure S32**).

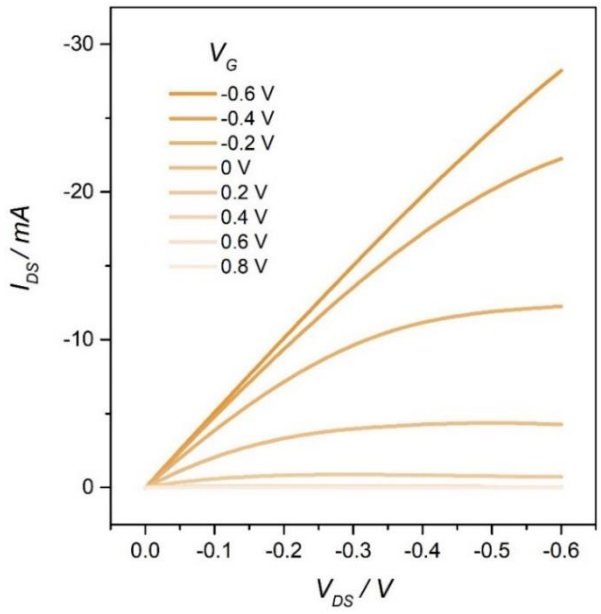

Figure S32. Output characteristics for a DBCO-HD22-modified PEDOT-N_3 OECT after thrombin (400 nM) sensing (1xPBS).

A comparison of the developed thrombin biosensing devices with other OECTs-based biosensors for relevant analytes is shown in **Table S3**.

Table S3. Comparison of OECTs-based biosensors.

Biosensing device	**Analyte**	**LOD**	**Reference**
AchE on PEDOT-PAH OECTs	Acetylcholine	5 μM	[17]
PEDOT:PSS OECTs	Dopamine	10 μM	[35]
PEDOT:PSS OECTs	Uric Acid	4.5 μM	[36]
LGluOx-PEDOT:PSS OECTs	Glutamate	5 μM	[37]
GOx-PEDOT:PSS OECTs	Glucose	1 μM	[38]
Congo red-PEDOT:PSS OECTs	Amyloid-β	1 fM	[39]
2,6-sialyllactose- PEDOT:PSS OECTs	Influenza A	0.025 HAU	[40]
Spike protein-PEDOT-PSS OECTs	SARS-CoV-2 IgG	10 fM	[41]
HD22-clicked PEDOT-N_3 OECTs	Thrombin	31 nM	***This work***

References

(1) Hasler, R.; Reiner-Rozman, C.; Fossati, S.; Aspermair, P.; Dostalek, J.; Lee, S.; Ibáñez, M.; Bintinger, J.; Knoll, W. Field-Effect Transistor with a Plasmonic Fiber Optic Gate Electrode as a Multivariable Biosensor Device. *ACS Sensors* **2022**, *7* (2), 504–512.

(2) Bu, H. B.; Götz, G.; Reinold, E.; Vogt, A.; Schmid, S.; Blanco, R.; Segura, J. L.; Bäuerle, P. "Click"-Functionalization of Conducting Poly(3,4- Ethylenedioxythiophene) (PEDOT). *Chem. Commun.* **2008**, No. 11, 1320–1322.

(3) Shavokshina, V. A.; Komkova, M. A.; Aparin, I. O.; Zatsepin, T. S.; Karyakin, A. A.; Andreev, E. A. Improved Electroactivity of Redox Probes onto Electropolymerized Azidomethyl-PEDOT: Enabling Click Chemistry for Advanced (Bio)Sensors. *ACS Appl. Polym. Mater.* **2021**, *3* (3), 1518–1524.

(4) Luo, S. C.; Ali, E. M.; Tansil, N. C.; Yu, H. H.; Gao, S.; Kantchev, E. A. B.; Ying, J. Y. Poly(3,4-Ethylenedioxythiophene) (PEDOT) Nanobiointerfaces: Thin, Ultrasmooth, and Functionalized PEDOT Films with in Vitro and in Vivo Biocompatibility. *Langmuir* **2008**, *24* (15), 8071–8077.

(5) Rivnay, J.; Leleux, P.; Sessolo, M.; Khodagholy, D.; Hervé, T.; Fiocchi, M.; Malliaras, G. G. Organic Electrochemical Transistors with Maximum Transconductance at Zero Gate Bias. *Adv. Mater.* **2013**, *25* (48), 7010–7014.

(6) Fenoy, G. E.; Bilderling, C.; Knoll, W.; Azzaroni, O.; Marmisollé, W. A. PEDOT:Tosylate-Polyamine-Based Organic Electrochemical Transistors for High-Performance Bioelectronics. *Adv. Electron. Mater.* **2021**, *7* (6), 2100059.

(7) Doris, S. E.; Pierre, A.; Street, R. A. Dynamic and Tunable Threshold Voltage in Organic Electrochemical Transistors. *Adv. Mater.* **2018**, *30* (15), 1–5.

(8) Kergoat, L.; Herlogsson, L.; Piro, B.; Pham, M. C.; Horowitz, G.; Crispin, X.; Berggren, M. Tuning the Threshold Voltage in Electrolyte-Gated Organic Field-Effect Transistors. *Proc. Natl. Acad. Sci.* **2012**, *109* (22), 8394–8399.

(9) Paudel, P. R.; Kaphle, V.; Dahal, D.; Radha Krishnan, R. K.; Lüssem, B. Tuning the Transconductance of Organic Electrochemical Transistors. *Adv. Funct. Mater.* **2020**, *2004939*, 1–12.

(10) Koklu, A.; Ohayon, D.; Wustoni, S.; Druet, V.; Saleh, A.; Inal, S. Organic Bioelectronic Devices for Metabolite Sensing. *Chem. Rev.* **2022**, *122* (4), 4581–4635.

(11) Fenoy, G. E.; Marmisollé, W. A.; Azzaroni, O.; Knoll, W. Acetylcholine Biosensor Based on the Electrochemical Functionalization of Graphene Field-Effect Transistors. *Biosens. Bioelectron.* **2020**, *148*, 111796.

(12) Yu, S.; Ratcliff, E. L. Tuning Organic Electrochemical Transistor (OECT) Transconductance toward Zero Gate Voltage in the Faradaic Mode. *ACS Appl. Mater. Interfaces* **2021**, *13* (42), 50176–50186.

(13) Ko, Y. H.; Kim, Y. H.; Park, J.; Nam, K. T.; Park, J. H.; Yoo, P. J. Electric-Field-Assisted Layer-by-Layer Assembly of Weakly Charged Polyelectrolyte Multilayers. *Macromolecules* **2011**, *44* (8), 2866–2872.

(14) Daugaard, A. E.; Hvilsted, S.; Hansen, T. S.; Larsen, N. B. Conductive Polymer Functionalization by Click Chemistry. *Macromolecules* **2008**, *41* (12), 4321–4327.

(15) Faria, G. C.; Duong, D. T.; Salleo, A. On the Transient Response of Organic Electrochemical Transistors. *Org. Electron.* **2017**, *45*, 215–221.

(16) Bernards, D. A.; Malliaras, G. G. Steady-State and Transient Behavior of Organic Electrochemical Transistors. *Adv. Funct. Mater.* **2007**, *17* (17), 3538–3544.

(17) Fenoy, G. E.; Bilderling, C.; Knoll, W.; Azzaroni, O.; Marmisollé, W. A. PEDOT:Tosylate-

Polyamine-Based Organic Electrochemical Transistors for High-Performance Bioelectronics. *Adv. Electron. Mater.* **2021**, *7* (6), 2100059.

(18) Musumeci, C.; Vagin, M.; Zeglio, E.; Ouyang, L.; Gabrielsson, R.; Inganäs, O. Organic Electrochemical Transistors from Supramolecular Complexes of Conjugated Polyelectrolyte PEDOTS. *J. Mater. Chem. C* **2019**, *7* (10), 2987–2993.

(19) Fenoy, G. E.; Giussi, J. M.; von Bilderling, C.; Maza, E. M.; Pietrasanta, L. I.; Knoll, W.; Marmisollé, W. A.; Azzaroni, O. Reversible Modulation of the Redox Activity in Conducting Polymer Nanofilms Induced by Hydrophobic Collapse of a Surface-Grafted Polyelectrolyte. *J. Colloid Interface Sci.* **2018**, *518*, 92–101.

(20) Bobacka, J.; Lewenstam, A.; Ivaska, A. Electrochemical Impedance Spectroscopy of Oxidized Poly(3,4-Ethylenedioxythiophene) Film Electrodes in Aqueous Solutions. *J. Electroanal. Chem.* **2000**, *489* (1), 17–27.

(21) Jacobsen, T.; West, K. Diffusion Impedance in Planar, Cylindrical and Spherical Symmetry. *Electrochim. Acta* **1995**, *40* (2), 255–262.

(22) Carli, S.; Bianchi, M.; Zucchini, E.; Di Lauro, M.; Prato, M.; Murgia, M.; Fadiga, L.; Biscarini, F. Electrodeposited PEDOT:Nafion Composite for Neural Recording and Stimulation. *Adv. Healthc. Mater.* **2019**, *8* (19), 1–10.

(23) Hopkins, J.; Fidanovski, K.; Travaglini, L.; Ta, D.; Hook, J.; Wagner, P.; Wagner, K.; Lauto, A.; Cazorla, C.; Officer, D.; et al. A Phosphonated Poly(Ethylenedioxythiophene) Derivative with Low Oxidation Potential for Energy-Efficient Bioelectronic Devices. *Chem. Mater.* **2022**, *34* (1), 140–151.

(24) Lieber, E.; Rao, C. N. R.; Hoffman, C. W. W.; Chao, T. S. Infrared Spectra of Organic Azides. *Anal. Chem.* **1957**, *29* (6), 916–918.

(25) Zhao, Q.; Jamal, R.; Zhang, L.; Wang, M.; Abdiryim, T. The Structure and Properties of PEDOT Synthesized by Template-Free Solution Method. *Nanoscale Res. Lett.* **2014**, *9* (1), 1–9.

(26) Sriprachuabwong, C.; Karuwan, C.; Wisitsorrat, A.; Phokharatkul, D.; Lomas, T.; Sritongkham, P.; Tuantranont, A. Inkjet-Printed Graphene-PEDOT:PSS Modified Screen Printed Carbon Electrode for Biochemical Sensing. *J. Mater. Chem.* **2012**, *22* (12), 5478–5485.

(27) Zheng, Y.; Chen, Y. Preparation of Polypropylene/Mg-Al Layered Double Hydroxides Nanocomposites through Wet Pan-Milling: Formation of a Second-Staging Structure in LDHs Intercalates. *RSC Adv.* **2017**, *7* (3), 1520–1530.

(28) Fenoy, G. E.; Rafti, M.; Marmisollé, W. A.; Azzaroni, O. Nanoarchitectonics of Metal Organic Frameworks and PEDOT Layer-by-Layer Electrodes for Boosting Oxygen Reduction Reaction. *Mater. Adv.* **2021**, *2* (23), 7731–7740.

(29) Fenoy, G. E.; Maza, E.; Zelaya, E.; Marmisollé, W. A.; Azzaroni, O. Layer-by-Layer Assemblies of Highly Connected Polyelectrolyte Capped-Pt Nanoparticles for Electrocatalysis of Hydrogen Evolution Reaction. *Appl. Surf. Sci.* **2017**, *416*, 24–32.

(30) Gao, X.; Chorover, J. Adsorption of Sodium Dodecyl Sulfate (SDS) at ZnSe and α-Fe2O3 Surfaces: Combining Infrared Spectroscopy and Batch Uptake Studies. *J. Colloid Interface Sci.* **2010**, *348* (1), 167–176.

(31) Baba, A.; Lübben, J.; Tamada, K.; Knoll, W. Optical Properties of Ultrathin Poly(3,4-Ethylenedioxythiophene) Films at Several Doping Levels Studied by In Situ Electrochemical Surface Plasmon Resonance Spectroscopy. *Langmuir* **2003**, *19* (21), 9058–9064.

(32) Vörös, J. The Density and Refractive Index of Adsorbing Protein Layers. *Biophys. J.* **2004**, *87* (1), 553–561.

(33) Knoll, W.; Liley, M.; Piscevic, D.; Spinke, J.; Tarlov, M. J. Supramolecular Architectures for the

Functionalization of Solid Surfaces. *Adv. Biophys.* **1997**, *34*, 231–251.

(34) Stenberg, E.; Persson, B.; Roos, H.; Urbaniczky, C. Quantitative Determination of Surface Concentration of Protein with Surface Plasmon Resonance Using Radiolabeled Proteins. *J. Colloid Interface Sci.* **1991**, *143* (2), 513–526.

(35) Tybrandt, K.; Kollipara, S. B.; Berggren, M. Organic Electrochemical Transistors for Signal Amplification in Fast Scan Cyclic Voltammetry. *Sensors Actuators B Chem.* **2014**, *195*, 651–656.

(36) Galliani, M.; Diacci, C.; Berto, M.; Sensi, M.; Beni, V.; Berggren, M.; Borsari, M.; Simon, D. T.; Biscarini, F.; Bortolotti, C. A. Flexible Printed Organic Electrochemical Transistors for the Detection of Uric Acid in Artificial Wound Exudate. *Adv. Mater. Interfaces* **2020**, *2001218*, 1–7.

(37) Kergoat, L.; Piro, B.; Simon, D. T.; Pham, M. C.; Noël, V.; Berggren, M. Detection of Glutamate and Acetylcholine with Organic Electrochemical Transistors Based on Conducting Polymer/Platinum Nanoparticle Composites. *Adv. Mater.* **2014**, *26* (32), 5658–5664.

(38) Macaya, D. J.; Nikolou, M.; Takamatsu, S.; Mabeck, J. T.; Owens, R. M.; Malliaras, G. G. Simple Glucose Sensors with Micromolar Sensitivity Based on Organic Electrochemical Transistors. *Sensors Actuators, B Chem.* **2007**, *123* (1), 374–378.

(39) Koklu, A.; Wustoni, S.; Musteata, V. E.; Ohayon, D.; Moser, M.; McCulloch, I.; Nunes, S. P.; Inal, S. Microfluidic Integrated Organic Electrochemical Transistor with a Nanoporous Membrane for Amyloid-β Detection. *ACS Nano* **2021**, *15* (5), 8130–8141.

(40) Hai, W.; Goda, T.; Takeuchi, H.; Yamaoka, S.; Horiguchi, Y.; Matsumoto, A.; Miyahara, Y. Human Influenza Virus Detection Using Sialyllactose-Functionalized Organic Electrochemical Transistors. *Sensors Actuators, B Chem.* **2018**, *260*, 635–641.

(41) Liu, H.; Yang, A.; Song, J.; Wang, N.; Lam, P.; Li, Y.; Law, H. K. W.; Yan, F. Ultrafast, Sensitive, and Portable Detection of COVID-19 IgG Using Flexible Organic Electrochemical Transistors. *Sci. Adv.* **2021**, *7* (38), 1–10.